Neurotherapeutics (2013) 10:520–538
DOI 10.1007/s13311-013-0198-1

ORIGINAL ARTICLE

Cell Cycle Activation Contributes to Increased Neuronal Activity in the Posterior Thalamic Nucleus and Associated Chronic Hyperesthesia after Rat Spinal Cord Contusion

Junfang Wu · Charles Raver · Chunshu Piao · Asaf Keller · Alan I. Faden

Published online: 18 June 2013

Abstract Spinal cord injury (SCI) causes not only sensorimotor and cognitive deficits, but frequently also severe chronic pain that is difficult to treat (SCI pain). We previously showed that hyperesthesia, as well as spontaneous pain induced by electrolytic lesions in the rat spinothalamic tract, is associated with increased spontaneous and sensory-evoked activity in the posterior thalamic nucleus (PO). We have also demonstrated that rodent impact SCI increases cell cycle activation (CCA) in the injury region and that post-traumatic treatment with cyclin dependent kinase inhibitors reduces lesion volume and motor dysfunction. Here we examined whether CCA contributes to neuronal hyperexcitability of PO and hyperpathia after rat contusion SCI, as well as to microglial and astroglial activation (gliopathy) that has been implicated in delayed SCI pain. Trauma caused enhanced pain sensitivity, which developed weeks after injury and was correlated with increased PO neuronal activity. Increased CCA was found at the thoracic spinal lesion site, the lumbar dorsal horn, and the PO. Increased microglial activation and cysteine–cysteine chemokine ligand 21 expression was also observed in the PO after SCI. *In vitro*, neurons co-cultured with activated microglia showed up-regulation of cyclin D1 and cysteine–cysteine chemokine ligand 21 expression. *In vivo*, post-injury treatment with a selective cyclin dependent kinase inhibitor (CR8) significantly reduced cell cycle protein induction, microglial activation, and neuronal activity in the PO nucleus, as well as limiting chronic SCI-induced hyperpathia. These results suggest a mechanistic role for CCA in the development of SCI pain, through effects mediated in part by the PO nucleus. Moreover, cell cycle modulation may provide an effective therapeutic strategy to improve reduce both hyperpathia and motor dysfunction after SCI.

Keywords Cell cycle activation · Posterior thalamic nucleus · Neuronal hyperexcitability · Pain · Hyperalgesia · Inflammation

Junfang Wu and Charles Raver contributed equally to this article.

J. Wu (✉) · C. Piao · A. I. Faden
Department of Anesthesiology & Center for Shock, Trauma and Anesthesiology Research (STAR), National Study Center for Trauma and EMS, University of Maryland, School of Medicine, Bressler Research Building, 655 W. Baltimore Street, Room #6-009, Baltimore, MD 21201, USA
e-mail: jwu@anes.umm.edu

C. Raver · A. Keller
Department of Anatomy and Neurobiology, University of Maryland School of Medicine, Baltimore, MD, USA

A. Keller · A. I. Faden
Program in Neuroscience, University of Maryland School of Medicine, Baltimore, MD, USA

Introduction

Traumatic spinal cord injury (SCI) is a leading cause of paralysis, and may lead to other catastrophic consequences, including compromised bladder and bowel functions [1], emotional and psychological distress [2], and loss of sexual function [3]. SCI results not only in debilitating motor and sensory, but also in chronic, hyperpathic pain (SCI pain). Such pain can be diffuse or bilateral, and often extends to locations caudal to the spinal injury ("below-lesion") [4–6]. Perhaps most debilitating is the presence in most patients of chronic, spontaneous pain [7, 8]. SCI pain is usually resistant

to treatment [9]. In most SCI patients chronic pain first appears more than 1 year after the injury [10–12]. The delayed expression of SCI pain, the diffuse localization of painful symptoms, and the presence of pain below the denervated spinal segment strongly suggest the occurrence of maladaptive plasticity not only in the spinal cord, but also in supraspinal structures [13]. The latent period between the spinal injury and the development of chronic pain provides a window of opportunity for interventions to prevent or minimize the development of SCI pain. Discovering new interventions to manage SCI pain requires a better understanding of the physiological mechanisms underlying the development of related maladaptive sensory plasticity after injury.

Chronic pain syndromes (CPS), including SCI pain, have long been suspected to involve the thalamus [14–16]. There are SCI-induced changes in several thalamic nuclei, including intralaminar, mediodorsal, ventral, and posterior nuclei [13, 17]. Activity of neurons and microglia in the ventroposteriolateral nucleus (VPL) appear to be abnormally increased in association with SCI pain [18–21]. The posterior nucleus (PO) of the thalamus receives convergent innocuous and noxious somatosensory inputs by way of the spinothalamic tract (STT), the major ascending pain pathway [22, 23]. We have previously reported increased spontaneous and sensory-evoked activity in PO that is associated with CPS induced by unilateral focal electrolytic lesions in the rat STT [24]. We also provided evidence that these changes are caused by reduced inhibitory inputs to PO, and that they are causally related to the experience of pain in these animals [13].

After SCI, chronic activation of microglia and astrocytes are found at the lesion site, caudal dorsal horn, and thalamus [21, 25–30]. Such changes have been implicated in the induction and maintenance of SCI pain. Identification of molecular mechanisms underlying this "gliopathy" [29, 31, 32] may therefore help to clarify the pathobiology of SCI pain and lead to the elucidation of novel therapeutic targets.

Cell cycle activation (CCA) contributes to both astroglial and microglial activation after central nervous system injuries, including SCI [33, 34]. In addition, cyclin dependent kinase (CDK) inhibitors can reduce neuronal death, suppress reactive glia, and improve neurological outcomes in a number of acute and chronic neurodegenerative disorders [33, 35–43]. Little is known about the role of cell cycle genes in neuropathic pain. Recently, the pan-CDK inhibitor, flavopiridol, administered intrathecally, was reported to reduce tactile allodynia after spinal nerve injury through inhibition of astrocyte proliferation [44]. Roscovitine, a more selective CDK inhibitor, reduced heat-induced hyperalgesia induced by complete Freund's adjuvant or formalin-induced nociceptive responses in rats [45, 46]. In the present study, we examined the effects of impact SCI in rats on the development of SCI pain, the potential role of the PO in mediating such pain, and whether CCA contributed to the development of post-traumatic hyperpathia and associated glial alterations.

Materials and Methods

All procedures were conducted according to Animal Welfare Act regulations and public health service (PHS) guidelines. Strict aseptic surgical procedures were used, according to the guidelines of the International Association for the Study of Pain, and approved by the University of Maryland School of Medicine Animal Care and Use Committee.

Spinal Cord Injury and Drug Administration

Adult male Sprague-Dawley rats weighing 275–325 g were anesthetized with sodium pentobarbital (65 mg/kg i.p.). Body temperature was kept by maintaining the animal on a heating pad (37 °C) throughout the procedure. Spinal contusion injury was produced at spinal segment T10 using our well-characterized rat impact injury device [30, 47]. A 10-g weight was dropped from a height of 2.5 cm onto the exposed spinal cord without disrupting the dura. Sham-injured rats received a laminectomy without trauma. Post-operatively, rats were injected subcutaneously with 5 ml of 0.9 % saline and allowed to recover on a heating pad. Bladders were manually expressed twice a day until reflex bladder emptying was established, typically by 10–14 d after injury. After SCI, rats were assigned to a treatment group according to a randomized block experimental design. The number of rats at various time points in each study is indicated in the figures legends. CR8 (Tocris Bioscience, Ellisville, MO, USA) was dissolved in sterile saline and administered intraperitoneally, once daily beginning 3 h post-injury and continuing for 7 days. Groups of rats received 1 mg/kg CR8 or the equivalent volume of saline. This dose of CR8 was based upon prior investigations in SCI model [30, 46]. In addition, we have reported that systemic flavopiridol treatment (1 mg/kg) administered daily for 1 week following SCI enhanced functional recovery [43]. We now have evidence that anti-apoptotic concentrations of CR8 in cultured cortical neurons were similar to those of flavopiridol, a potent pan-CDK inhibitor. The effect of CR8 on microglial proliferation and activation in response to LPS in cultured primary microglia was also similar to that of flavopiridol.

Behavioral Assessments

Open-Field Test (Basso, Beattie, and Bresnahan Scores)

Rats were assessed for hind limb function in open field locomotion on day 1 post-injury and weekly thereafter for up to 5 weeks, using the Basso, Beattie and Bresnahan (BBB) open field expanded locomotor score [48].

Combined Behavioral Score

Neurological functional deficits were also estimated with a combined behavioral score (CBS), which included open field locomotion (motor score); withdrawal reflex to hind limb extension, pain and pressure; foot placing, toe spread and righting reflexes; maintenance of position on an inclined plane; and swimming tests [49].

Hind Paw Mechanical Withdrawal Thresholds

All animals were tested on 3 consecutive days before the SCI, at day 21 after surgery, and at weekly intervals thereafter, until electrophysiological data were collected. To minimize the animals' anxiety they were habituated for 2 days before behavioral testing. Mechanical withdrawal thresholds were measured using the Dynamic Plantar Aesthesiometer (Ugo Basile, Comerio, VA, Italy) at a ramp speed of 5 g/s. Force at the time of paw withdrawal was measured over 3 trials on a testing day for each hindpaw and averaged. Post-surgery percent change in thresholds from baseline was calculated for each hindpaw and averaged for a bilateral measure of algesia for each animal.

Extracellular Recordings

At least 45 days after SCI, rats were anesthetized with urethane and prepared for extracellular recordings as previously described [24, 50]. We selected urethane because it has no, or negligible, effects on glutamatergic and gamma-aminobutryic acid (GABA)ergic transmission, and therefore produces only minimal disruption of signal transmission [51]. We administered 20 % urethane intraperitoneally at intervals to maintain the animal at level III-2, as described by Friedberg et al. [52] with a total dose not exceeding 1.5 mg/kg. Anesthetic levels were monitored continually using respiration rate; vibrissae movement; and hindpaw pinch, corneal, and eyelid reflexes.

Extracellular recordings were obtained from PO thalamus through quartz-insulated tungsten electrodes (1–4 MΩ). We recorded from well-isolated units, digitized (40 kHz) the waveforms through a Plexon (Dallas, TX, USA) data-acquisition system, and sorted units off-line with Plexon's off-line sorter, using dual thresholds and principle component analyses. We generated autocorrelograms with Neuroexplorer software (Plexon) to confirm that we obtained recordings from single units. We exported time stamps of well-isolated units and stimulus triggers to Matlab (MathWorks, Natick, MA, USA) for analyses using custom-written algorithms.

Tissue Processing and Histopathology

At specific times after injury, rats were deeply anesthetized with sodium pentobarbital (100 mg/kg i.p.) and transcardially perfused with 200 ml of normal saline followed by 500 ml of PBS containing 4 % paraformaldehyde (PH 7.4). The brain and spinal cord were removed, postfixed in 4 % paraformaldehyde overnight, and transferred to 30 % sucrose at 4 °C. Coronal sections were cut with a cryostat and thaw-mounted onto Superfrost Plus slides (Fisher Scientific, Pittsburg, PA, USA).

Assessment of White Matter Sparing

Every twentieth slide from each set was stained with eriochrome cyanine (ECRC) and residual white matter (WM) area was calculated at the injury epicenter, as well as at points rostral and caudal to the epicenter by quantifying the total area stained by ECRC. Images were taken at 2.5× magnification and analyzed using NIH ImageJ software. The threshold level of each 8-bit image was set to display only ECRC-positive pixels, and total ECRC-positive area was calculated for each section.[43] The lesion epicenter was defined as the section with the least amount of spared WM.

Estimation of Lesion Volume

Lesion volume was assessed using the Stereologer 2000 software (Systems Planning and Analysis, Alexandria, VA, USA) [30]. Sections spaced 1 mm apart from 5 mm caudal to 5 mm rostral the injury epicenter were stained with glial fibrillary acidic protein (GFAP) and diaminobenzidine (DAB) as the chromogen for lesion volume assessment based on the Cavalieri method of unbiased stereology with a grid spacing of 200 μm.

Stereological Quantification of Microglial Phenotypes

StereoInvestigator Software (MBF Biosciences, Williston, VT, USA) was used to count the number of the three microglial morphological phenotypes (ramified, hypertrophic, and bushy) in both the lesion and spared tissue using the optical fractionator method of unbiased stereology [53]. Spinal cord sections from the 7-d rat study, spaced 1 mm apart from 5 mm caudal to 5 mm rostral the injury epicenter, were stained for ionized calcium-binding adaptor molecule 1 (Iba-1) and DAB. Contours outlining spared and lesion tissue were traced onto each section, based on GFAP staining of adjacent sections. The optical dissector had a size of 50 μm×50 μm, a height of 10 μm, and a guard zone of 4 μm from the top of the section. A grid spacing of 250 μm in the x-axis and 250 μm in the y-axis was used. Microglia were counted throughout both spared and lesion tissue. Microglial phenotypic classification was based on the length and thickness of the projections, the number of branches and the size of the cell body, as previously described [54, 55]. The volume of the region of interest was measured using Cavalieri estimator method. The

estimated number of microglia in each phenotypic class was divided by the volume of the region of interest to obtain the cellular density expressed in counts/mm^3. Neurolucida software (MBF Biosciences) was used to create reconstructions of microglia at different stages of activation after injury by tracing the cell bodies and dendrites [55]. Microglia were outlined using the live image setting so that the width of the dendrites could be traced while focusing on the section. The cell bodies were outlined using the contour tool followed by tracing of individual dendrites, using the dendrite line tool.

Stereology and GFAP$^+$ Cell Counts

Eight or nine representative subjects (based on BBB score) from the 5-week rat study were selected from each treatment group for quantification of astrocytes (GFAP$^+$ cells) using the optical fractionator method with the aid of StereoInvestigator Software. Sections spaced 1 mm apart from 5 mm caudal to 5 mm rostral the injury epicenter were included for counting [43]. A sampling grid comprised of 250 μm×250 μm squares (150 μm×150 μm squares in the gray matter for GFAP$^+$ cells) was laid over each section. Cells were counted in a 50 μm×50 μm counting frame within each square of the counting grid with a height of 10 μm and a guard zone of 4 μm from the top of the section. GFAP$^+$ cells were counted throughout the entire section.

Immunofluorescent Staining and Quantification

Immunohistochemistry was performed on brain and spinal cord coronal sections at specified distances rostral and caudal to the injury epicenter. Standard fluorescent immunocytochemistry on serial, 20-μm thick sections was performed as described previously [56]. The following primary antibodies were used: rabbit anti-Iba-1 (1:1000; Wako Chemicals, Richmond, VA, USA), mouse anti-cyclin D1 (1:500; Neomarker, Fremont, CA, USA), rabbit anti- cysteine–cysteine chemokine ligand (CCL)21 (1:200; Abcam, Cambridge, MA, USA), mouse anti-CD68 (ED1, 1:500; AbDerotec, Raleigh, NC, USA). Fluorescent-conjugated secondary antibodies (Alexa 488-conjugated goat anti-mouse or rabbit, 1:1000; Molecular Probes, Grand Island, NY, USA) were incubated with tissue sections for 1 h at room temperature. Cell nuclei were labeled with 4', 6-diamidino-2-phenylindole (1 μg/ml; Sigma, St. Louis, MO, USA). Finally, slides were washed and mounted with an anti-fading medium (Invitrogen, Grand Island, NY, USA). Immunofluorescence microscopy was performed using a Leica TCS SP5 II Tunable Spectral Confocal microscope system (Leica Microsystems, Bannockburn, IL, USA). The images were processed using Adobe Photoshop 7.0 software (Adobe Systems, San Jose, CA, USA). All immunohistological staining experiments were carried out with appropriate positive control tissue, as well as primary/secondary-only negative controls.

For quantitative image analysis, digital images at 20× magnification were captured from the PO, VPL, ventral posteromedial (VPM), and centrolateral (CL) nuclei, based on atlas boundaries and using a confocal laser-scanning microscope (n=3 sections/location/time point/rat for 6–8 rats/group). These were analyzed to quantify Iba-1- and cyclin D1-expressing cells with ImageJ software (1.43; NIH, Bethesda, MD, USA). Based on the gray values of digital images, the threshold was set to display only fluorescence-positive pixels. Positive pixels of units of cell size (>7 μm diameter) were counted to estimate number of positive cell-sized particles [21, 57]. In addition, the number of ED1$^+$/Iba-1$^+$ cells were counted for each animal by an average of bilateral counts on each of 2 spinal cord sections (4 samples) at a predefined area of superficial lumbar dorsal horn.

Western Blots

Animals were deeply anesthetized with sodium pentobarbital (100 mg/kg i.p.), and spinal cord tissue (5 mm) centered on the injury site was removed and stored at –80 °C for processing. The tissue was homogenized (a glass on glass) and sonicated in radioimmunoprecipitation assay buffer (Sigma), and then centrifuged at 20,600×g for 20 min at 4 °C. The supernatant was removed and protein concentration was determined using the Pierce BCA Protein Assay kit (Thermo Scientific, Rockford, IL, USA) with a bovine serum albumin standard. Each sample contained proteins from one animal. Equal amounts of protein were electrophoretically separated on 4–12 % NuPAGE Novex Bis-Tris gradient gels (Invitrogen) and transferred to nitrocellulose membranes (Invitrogen). After blocking in 5 % nonfat milk for 1 h at room temperature, membranes were incubated with respective antibodies against cysteine–cysteine chemokine ligand 21 (CCL21) (polyclonal, 1:500; Abcam), CDK4 (polyclonal, 1:1,000; Santa Cruz Biotechnology, Santa Cruz, CA, USA), cyclin D1 (polyclonal, 1:500; Neomarker), cyclin E (monoclonal, 1:500; Santa Cruz Biotechnology), galectin 3 (monoclonal, 1:1000; Abcam), ionized calcium-binding adaptor molecule 1 (polyclonal, 1:1,000; Wako Chemicals), GFAP (monoclonal, 1:10,000; Chemicon, Billerica, MA, USA), and proliferating cell nuclear antigen (PCNA) (polyclonal, 1:500; Santa Cruz Biotechnology) overnight at 4 °C followed by horseradish peroxidase-conjugated secondary antibodies (GE Healthcare, Sykesville, MD, USA) for 1.5 h at room temperature. The immunoreactivity was detected using SuperSignal West Dura Extended Duration Substrate (Thermo Scientific), and quantified by band densitometry of scanned films using the Gel-Pro Analyzer program (Media

Cybernetics, Gaithersburg, MD, USA). Some blots were further stripped in a stripping buffer (Thermo Scientific) for 45 min at 55 °C. The loading and blotting of equal amounts of protein were verified by re-probing the membrane with anti-glyceraldehyde 3-phosphate dehydrogenase (monoclonal, 1:1000; Chemicon).

Primary Microglia Culture and Conditioned Medium Preparation

Primary microglia were cultured from the cerebral cortex of 1–3-day-old rats as described [58]. In brief, cerebra were dissected and chopped with microscissors. After incubation with 0.125 % trypsin/ethylenediaminetetraacetic acid for 10 min at 37 °C, the tissue was triturated and centrifuged at 500×*g* for 10 min. The resulting cell suspension was plated on 150 cm^2 tissue culture flasks that had been coated with poly-d-lysine (50 μg/ml, 70–150 kDa). The cells were grown in Dulbecco's Modified Eagle's Medium/F12 (Invitrogen) supplemented with 10 % fetal bovine serum (Invitrogen), 1 % Pen/Strep at 37 °C with 5 % carbon dioxide. When the cells had grown to confluence, the flasks were shaken at 100 rpm for 1 h at 37 °C to isolate microglia. Then, the cells were re-plated in 3.5 cm dishes. When microglia had reached confluence, lipopolysaccharide (LPS) (50 ng/ml) was applied to the dish for 24 h. Cells were then washed twice with pre-warmed PBS, and the culture medium was replaced. After a 2-day culture period, the medium was collected and filtered to be used as conditioned culture medium.

Primary Cortical Neuronal Culture

Rat primary cortical neuronal cultures were derived from E18 rat cortices, as previously described [56]. Cells were seeded at a density of 1×10^6 cells/cm^2 onto poly-d-lysine-coated 6-well plates. Arabinofuranosyl cytidine was added 24 h after plating (5 μM). The culture was maintained in serum-free conditions using Neurobasal medium supplemented with 2 % B27, 25 mM Na-glutamate, and 0.5 mM L-glutamine. Conditioned media harvested from the stimulated microglia was added to the

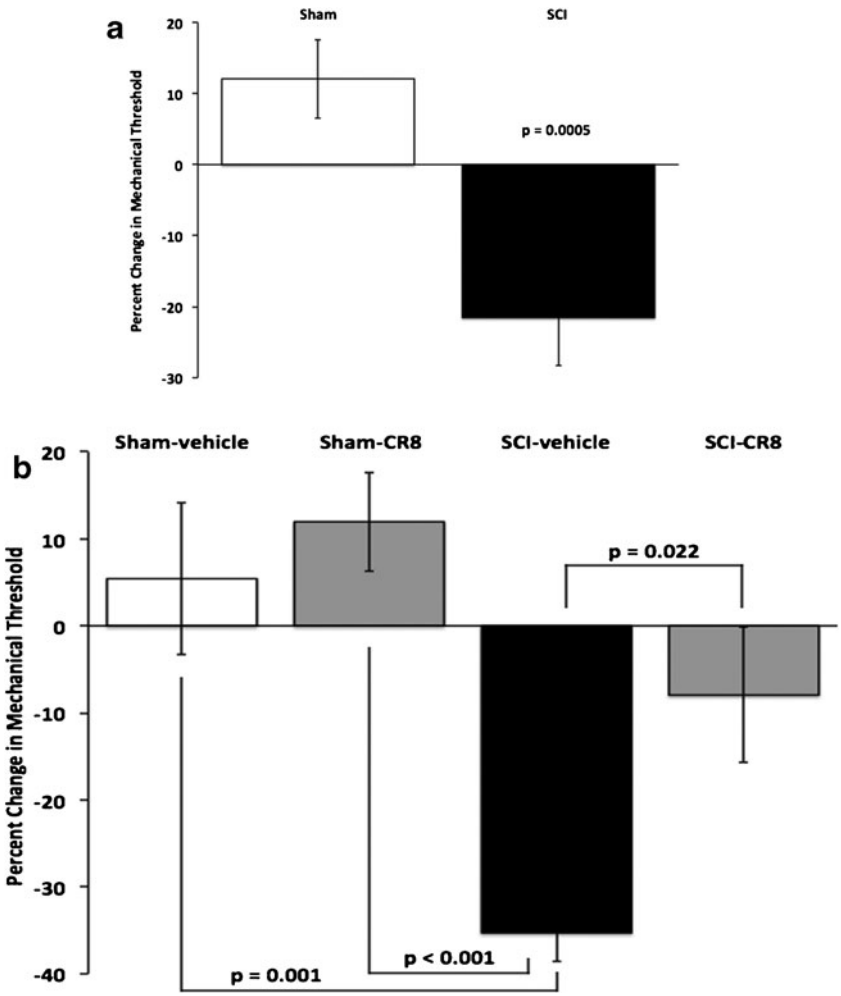

Fig. 1 Contusion spinal cord injury causes mechanical hyperesthesia. (**a**) Spinal cord injury (SCI) (n=16 animals) resulted in a significant (p=0.0005, t test) decrease from baseline in withdrawal thresholds to mechanical stimuli compared with sham controls (n=12). (**b**) Treatment with the cell-cycle inhibitor CR8 significantly (p<0.001) attenuated the development of hyperesthesia after SCI. One-way analysis of variance with Bonferroni adjustment revealed that SCI vehicle-treated animals (n=12) were significantly different from SCI animals treated with CR8 (p=0.022, n=11) and sham controls (vehicle, p=0.001, n=9; CR8, p<0.001, n=13). No other between-group differences were significant. Note that data in panels (**a**) and (**b**) are derived from different experimental groups

cultured neurons at 7 days *in vitro* for a further 48 h. Whole-cell extracts were prepared for Western blotting, as described previously [58].

Microglia Proliferation Assay

In vitro cell proliferation was assessed in microglia cultures by using a microculture [3-(4,5-dimethylthiazol-2-yl)-2,5-diphenyltetrazolium bromide (Sigma)]-based colorimetric assay. Briefly, freshly purified cells were plated at 30,000 cells/well in a 96-well plate. After pre-treatment for 1 h with CR8, roscovitine (Tocris Bioscience, Ellisville, MO, USA), flavopiridol (Santa Cruz Biotechnology), or vehicle, the cells were stimulated with LPS 50 ng/ml for 24 h. 3-(4,5-dimethylthiazol-2-yl)-2,5-diphenyltetrazolium bromide was added to cell cultures to give a final concentration 357 μg/ml, and the samples were incubated for 2 h at 37 °C in 5 % carbon dioxide. The supernatant was then removed and the formazan crystals produced in viable cells were solubilized with 150 μl dimethyl sulfoxide. Finally, the absorbance of each well was read at 570 nm using a microplate reader.

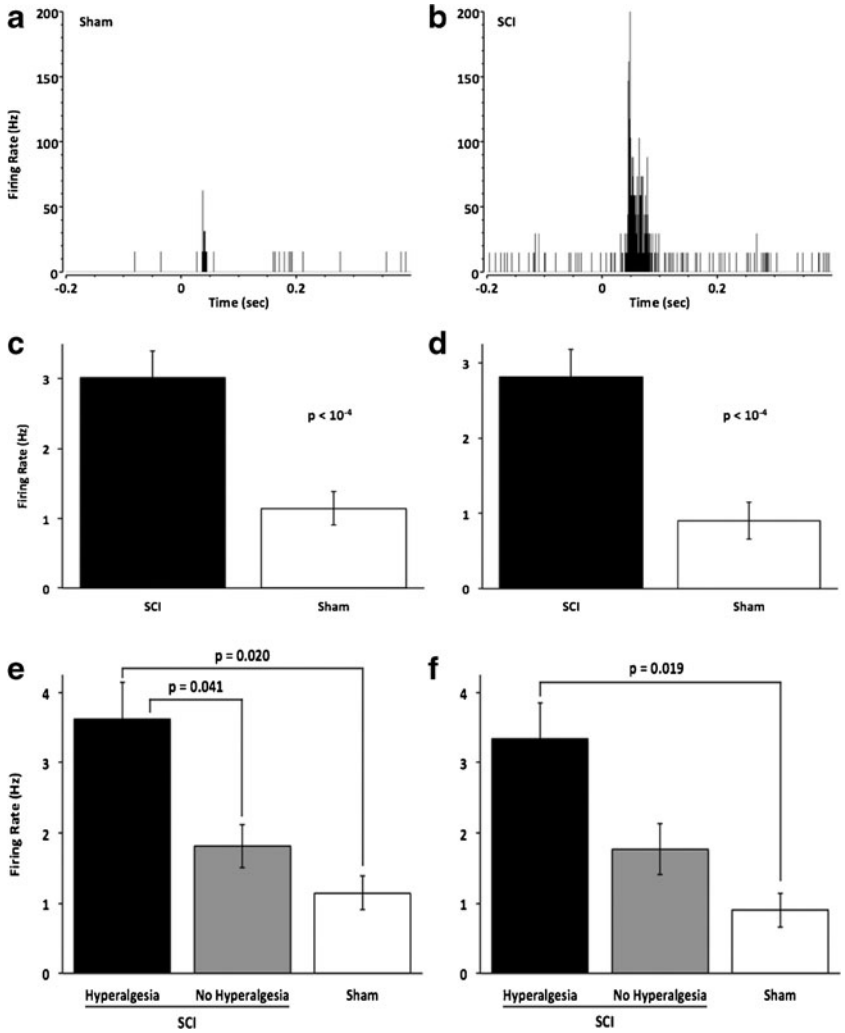

Fig. 2 Contusion spinal cord injury results in increased neuronal activity in the posterior thalamic nucleus (PO). (**a**, **b**) Representative peristimulus time histograms (1 ms bins) demonstrate that both spontaneous neuronal activity (activity before=0) and activity in response to a sensory stimulus (delivered at t=0) is elevated in spinal cord injury (SCI) animals (**b**) compared with sham controls (**a**). (**c**, **d**) Group data show that spontaneous (**c**) and sensory-evoked (**d**) firing rates are significantly higher in SCI animals (n=81 cells) than in shams (n=15). (**e**, **f**) Spontaneous and sensory-evoked neuronal activity is highest in those animals with clear hyperesthesia. One-way analysis of variance with Bonferroni correction revealed that spontaneous activity (**e**) was significantly (p=0.0053) higher after SCI, as well as in animals with hyperesthesia (n=54 cells), compared with those without hyperesthesia (p=0.041, n=27) and sham control (p=0.02, n=15), but not between those without hyperesthesia and sham operations. Similarly, sensory-evoked activity (**f**) is increased significantly (p=0.0084) after SCI. PO activity in SCI animals with hyperesthesia was significantly higher compared with shams (p=0.019), whereas activity in animals without hyperesthesia was not significantly higher compared with that in animals with hyperesthesia or in shams

Nitric Oxide Assay

The nitrite in the culture supernatant was measured as an indicator of nitric oxide (NO) production using the Griess reagent assay (Invitrogen), according to the manufacturer's instructions.

Data Analysis

Unless indicated otherwise, results are expressed as mean ± SEM, where "n" is the number of individual animals. Statistical comparisons included two-way analysis of variance (ANOVA) with repeated measures in behavioral experiments, Student's *t* test or one-way ANOVA with the Tukey or Newman-Keuls post-hoc test in lesion volume, WM sparring, cell counting, and Western blot analysis. All statistical analyses were conducted by using the GraphPad Prism Program, Version 3.02 for Windows (GraphPad Software, La Jolla, CA, USA). In all cases, $p<0.05$ was considered statistically significant.

Results

Administration of CDK Inhibitor CR8 Reduces SCI-Induced Hyperesthesia

To test for SCI pain, the threshold of rats' responses to mechanical stimuli applied to the plantar surface of the hindpaw was examined. Testing began 3 or more weeks after SCI because in both humans and rodents with SCI, SCI pain develops after a latent period [11, 28, 35, 41]. As seen in Fig. 1(a), there was a significant ($p=0.0005$; *t* test) decrease in the threshold for withdrawal from mechanical stimuli of SCI animals (mean decrease=–21.5±6.7 %, n=16). In contrast, the thresholds of sham-operated controls did not change significantly (mean=12.1±5.5 %, n=12). To estimate the incidence of animals that developed SCI pain, we defined hyperalgesic states as decreases in withdrawal threshold that exceed 20 % of mean baseline values. Using this criterion, 63 % (10 of 16) of the animals developed SCI pain, a value similar to that reported in previous studies using similar approaches [17, 59, 60]. These values likely underestimate the extent and incidence of hyperesthesia because SCI animals had severe motor deficits (described below) that hinder their ability to withdraw from mechanical stimuli.

To test the potential prophylactic effect of cell cycle inhibition on the development of post-injury hyperesthesia, we systemically administered CR8 to a separate group of SCI animals [30, 56]. CR8 treatment significantly improved behavioral outcomes (Fig. 1b). The percent change in withdrawal thresholds in SCI animals that received CR8 (mean=–7.9±7.8 %, n=11) was statistically indistinguishable ($p=0.17$) from that of sham-operated rats that also received CR8 (mean=11.9±5.7 %, n=13), suggesting that CR8 treatment provided protection from the development of SCI pain. Consistent with this conclusion, the percent change in withdrawal threshold of SCI animals that received CR8 was significantly ($p=0.02$) lower than that in SCI rats that received vehicle injections (mean=–35.3±3.3 %, n=12). Further, there was a significant, negative correlation ($p=0.02$; Pearson's X^2) between the presence of hyperesthesia (defined as a >20 % decrease in threshold) and CR8 treatment: Hyperesthesia was less common in SCI animals that received CR8 (36 %; 4 of 11) than in SCI rats that received vehicle injections (83 %; 10 of 12). Administration of CR8 to sham-operated rats (n=13) had no significant effect on their withdrawal thresholds compared with those receiving vehicle injections ($p=1.0$). These findings demonstrate that inhibition of the cell cycle pathway by CR8 limits posttraumatic hyperesthesia.

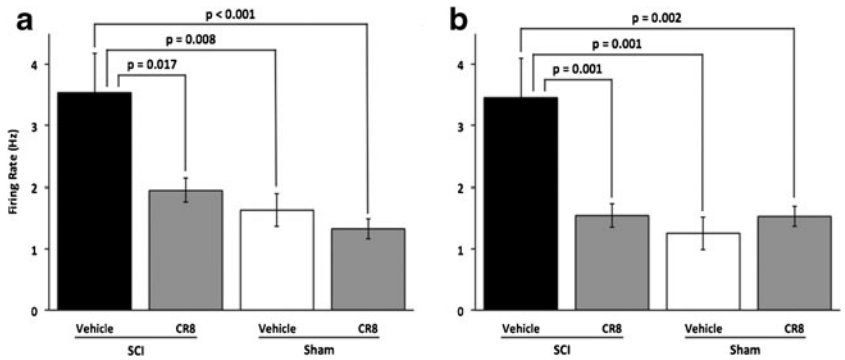

Fig. 3 Treatment with the cell cycle inhibitor CR8 attenuates the effects of contusion SCI on neuronal activity in posterior nucleus. Group data show a significant effect of treatment on both spontaneous (**a**, $p=0.0004$) and sensory-evoked activity (**b**, $p=0.0001$). (**a**) One-way analysis of variance with Bonferonni correction revealed that spontaneous firing rates in spinal cord injury (SCI) animals with vehicle treatment (n=33 cells) were significantly higher than those in SCI animals treated with CR8 ($p=0.017$, n=35 cells) and sham animals (vehicle, $p=0.008$, n=24; CR8, $p<0.001$, n=30). However, activity in SCI animals receiving CR8 was not significantly different from either sham group. (**b**) Similarly, evoked firing rates were significantly higher in SCI vehicle animals than those in SCI CR8 animals ($p=0.001$) and sham (vehicle, $p=0.001$; CR8, $p=0.002$). There was no difference between firing rates from SCI CR8 and either sham treatment condition

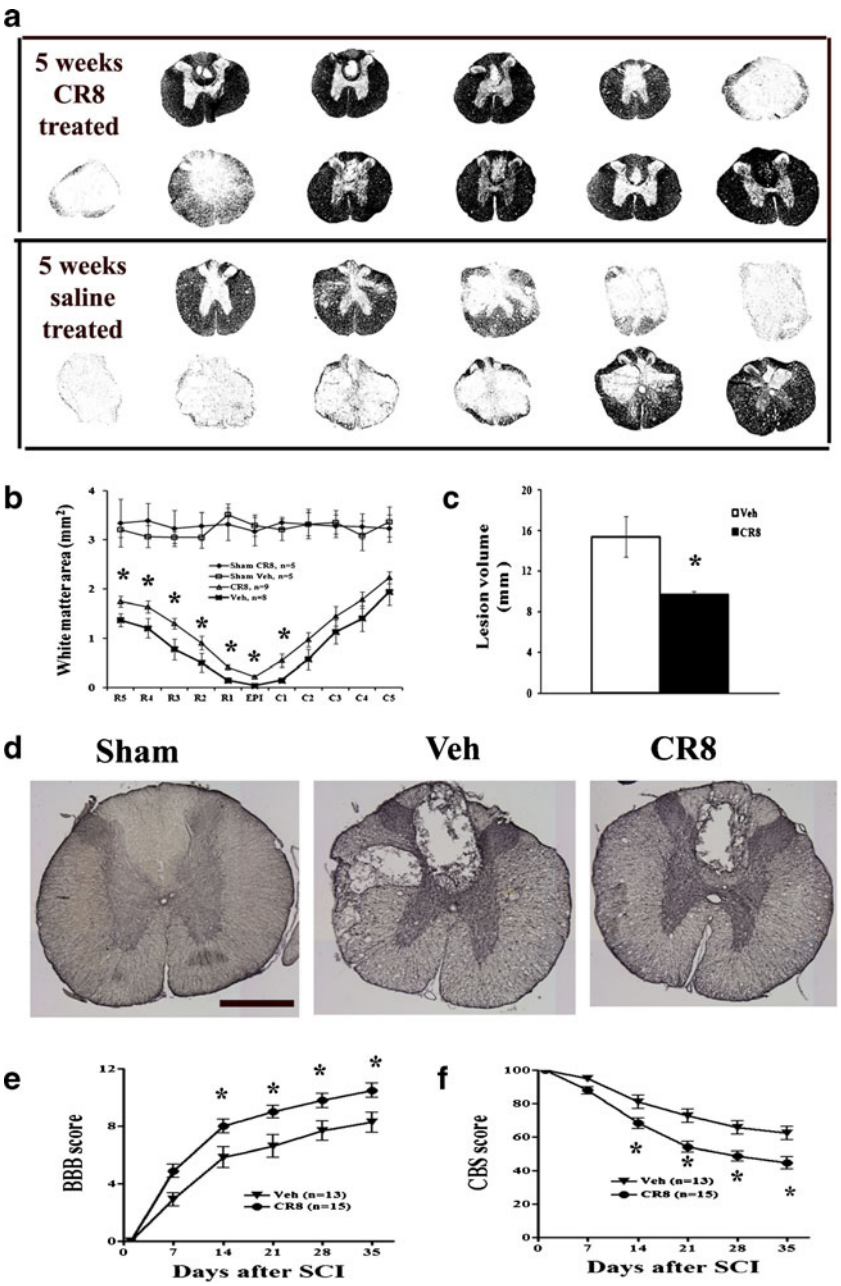

Fig. 4 Cell cycle inhibition increases white matter sparring, reduces lesion volume, and favors functional recovery after spinal cord injury (SCI). (**a**) A series of representative eriochrome stained tissue sections from CR8- or saline-treated rats at the epicenter and rostral (R1–R5) and caudal (C1–C5) to the injury epicenter (Epi). Eriochrome stains myelinated areas of spared white matter. (**b**) Quantification of the total white matter area (mm^2) in stained tissue sections from CR8-treated (n=10) and saline-treated rats (n=8). (**c**) The lesion volumes of CR8-treated rats (9.63±0.37 mm^3, n=10) are significantly smaller compared with saline-treated rats (15.40±2.00 mm^3, n=8) at 5 weeks after SCI. (**d**) Representative histologically stained tissue sections at 1 mm rostral to the epicenter from a sham rat and from injured saline- or CR8-treated rats. The SCI lesion is visible as a region with absence of glial fibrillary acidic protein/diaminobenzidine staining than the surrounding tissue. Scale bars=500 μm. (**e**, **f**) Neurological outcome was also evaluated using the Basso, Beattie and Bresnahan (BBB) score of hind limb locomotor function and the combined behavioral score (CBS), an evaluation of overall hind limb sensory-motor deficits. Both BBB and CBS tests showed significantly improved functional recovery in CR8-treated rats (n=15) compared with saline-treated rats (n=13). *$p<0.05$ compared with saline-treated group

Neuronal Activity in Thalamic PO is Increased After Spinal Cord Contusion and Reversed by CDK Inhibition

To further examine the role of cell-cycle activation in post-traumatic hyperesthesia and the development of SCI pain, we examined the effects of impact SCI and CR8 treatment on PO electrophysiology. We obtained single-unit, electrophysiological recordings from urethane-anesthetized rats, as previously described [24, 50, 61]. Consistent with our previous findings after electrolytic lesions of the spinothalamic tract [13], SCI significantly increased both spontaneous and sensory-evoked responses of PO neurons, as evidenced by comparing peri-stimulus time histograms (Fig. 2a, b). Group comparisons show that spontaneous firing rates of PO neurons in SCI rats (Fig. 2c; 3.0±0.4 Hz, n=81 neurons) are significant, and nearly 3-fold higher ($p<10^{-4}$, *t* test) than those in sham-operated controls (1.1±0.2 Hz, n=15). Using our previous criterion for the presence of hyperesthesia (see above), comparisons of SCI rats with or without post-injury hyperesthesia, and sham-operated controls, showed significant differences ($p=0.005$, one-way ANOVA with Bonferroni correction) in PO spontaneous activity (Fig. 2e). Between-group comparisons revealed a significant difference not only between SCI rats with hyperesthesia and sham-operated

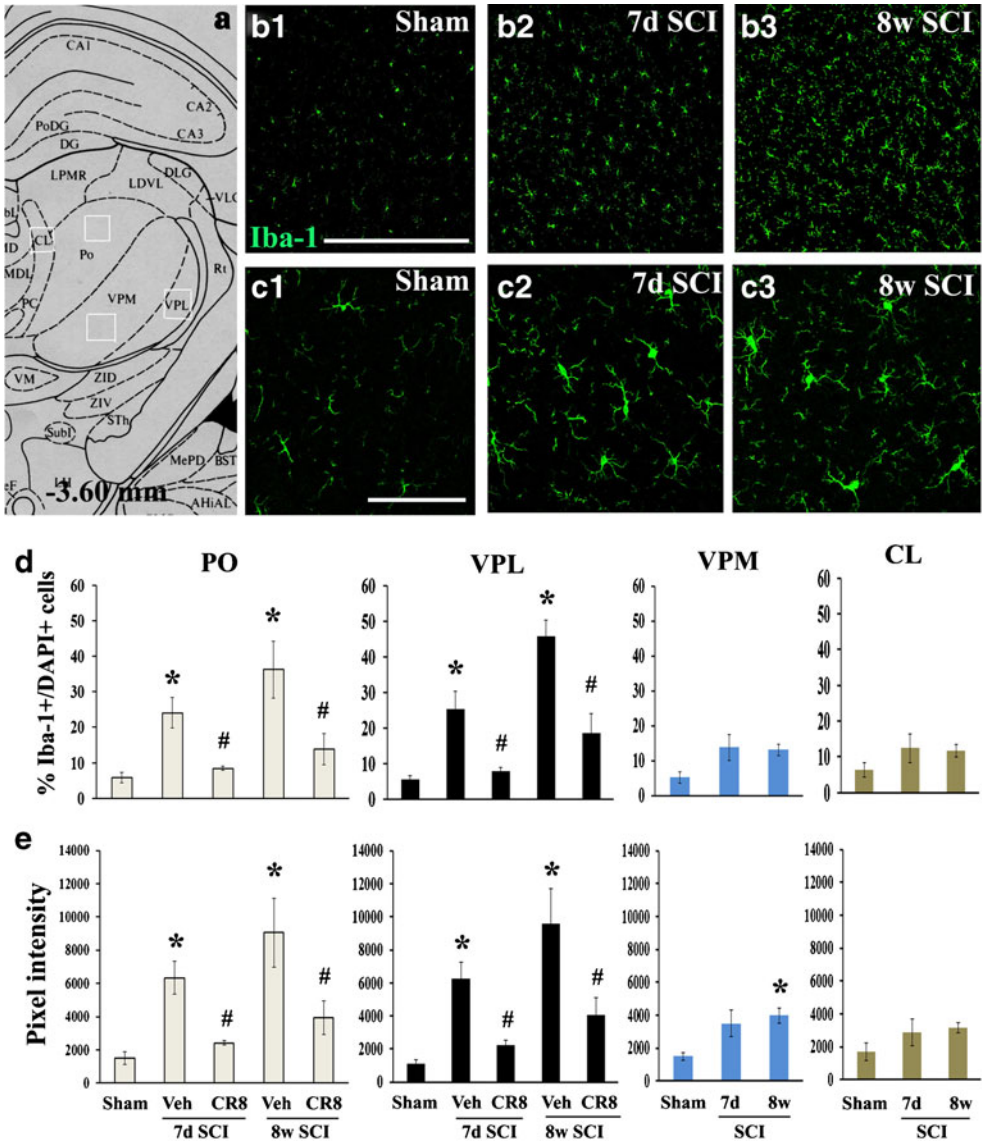

Fig. 5 Microglial activation in the posterior nucleus (PO) is progressive after spinal cord injury (SCI) and attenuated by cyclin dependent kinase (CDK) inhibition. (**a**) Approximate positions of relevant anatomical structures are shown in an atlas overlay [87]. (**b**) ionized calcium-binding adaptor molecule 1 (Iba-1) immunostaining revealed the presence of microglia in the PO of intact rat (b1). The number of Iba-1^{+} microglia at 7 days (7d) (b2) and 8 weeks (8w) (b3) post-injury was increased. (**c**) Microglia in the intact tissue displayed small compact somata bearing long thin ramified processes (c1) and exhibited larger cell body with shorter and thicker projections, and retraction of processes at 7 days (c2) and 8 weeks (c3) post-injury. (**d**) The percentage of Iba-1^{+} cells showed a significant increase in both PO and ventroposteriolateral nucleus (VPL) at 7 days and 8 weeks post-injury. This change was not observed in the adjacent centrolateral (CL) and ventral posteromedial (VPM) nucleus after SCI. CR8 treatment significantly reduced the number of Iba-1^{+} cells in the PO, as well as VPL, at both time points. (**e**) Quantification of pixel intensity for Iba-1 revealed significant microglial activation in both PO and VPL at 7 days and 8 weeks post-injury, as well as in the VPM at 8 weeks after SCI. These changes were remarkably suppressed by CR8 treatment. Microglial activation was not observed in the adjacent CL nucleus after SCI. n=3 sections/location/time point/rat for 6–8 rats/group. *p<0.05 *vs* Sham control; #p<0.05 *vs* vehicle (Veh) groups. Scale bars=500 μm for (**b**), and 100 μm for (**c**) and (**d**). *CA1-3* (fields CA1-3 of Ammon's horn); *DG* (dentate gyrus); *PoDG* (polymorph layer dentate gyrus); *LPMR* (lat post thal nu, mediorostral); *LDVL* (laterodorsal thal nu, ventrolat); *DLG* (dorsal lateral geniculate nu); *MDL* (mediodorsal thal nu, lateral); *Rt* (reticular thal nu); *PC* (paracentral thal nu); *VM* (ventromedial hypoth nu); *ZID* (zona incerta, dorsal); *ZIV* (zona incerta, ventral); *STh* (subthalamic nu); *Subl* (subincertal nu); *MePD* (medial amyg nu. posterodorsal)

controls (p=0.020), but also between the two SCI groups (p=0.041), with a significant negative correlation between PO firing rates and percent change in mechanical withdrawal thresholds (Pearson's r=–0.29, p=0.004). Responses to innocuous tactile stimuli were also significant, and approximately 4-fold higher ($p<10^{-4}$, *t* test) in SCI rats (Fig. 2d; 2.8±0.4 Hz, n=80) than shams (Fig. 2d; 0.7±0.1 Hz, n=15). Again, comparing responses from rats with or without post-traumatic hyperesthesia and those from sham-operated controls showed statistically significant differences (Fig. 2f; p=0.0084) with a

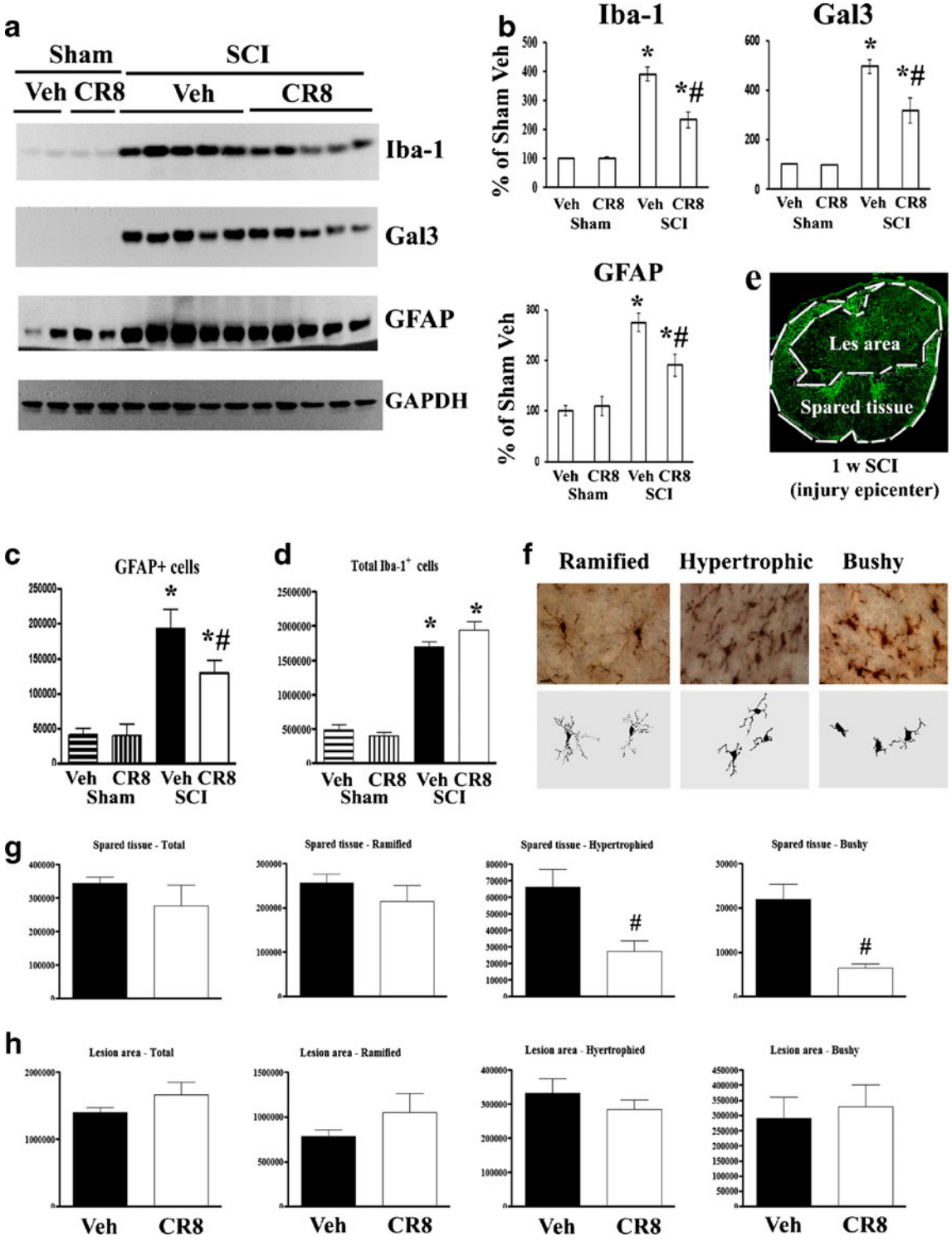

significant correlation between firing rates and percent change in baseline mechanical thresholds (Pearson's r=–0.26, p=0.0097). Thus, contusion SCI produces similar abnormalities in PO thalamus as those seen after selective electrolytic lesion of the spinothalamic tract [24], consistent with the hypothesis that changes of thalamic activity are causally related to development of SCI pain [13, 62].

To test the effect of cell cycle inhibition on the development of thalamic abnormalities, we compared spontaneous firing rates of PO neurons from 4 groups: rats with SCI that received CR8 treatment or vehicle injections, and sham-operated rats that received either CR8 or vehicle (Fig. 3). Spontaneous firing rates were significantly (p=0.017; Fig. 3a) lower in the SCI group that received CR8 (1.9±0.2 Hz, n=35

◀ **Fig. 6** Spinal cord injury (SCI)-induced astrogliosis and inflammation at the injury site are suppressed by CR8 treatment. (**a**, **b**) Western blot analysis shows that CR8 significantly reduced the SCI-induced up-regulation of ionized calcium-binding adaptor molecule 1 (Iba-1), gelectin3, and glial fibrillary acidic protein (GFAP) protein at 5 weeks post-injury. Representative immunoblots are shown in (**a**). *$p<0.05$ compared with Sham group (n=4 for Sham groups); #$p<0.05$ compared with SCI vehicle (Veh) group (n=5 for SCI groups). (**c**) GFAP-positive cells were significantly increased at 5 weeks post-injury in both saline- (n=8) and CR8-treated rats (n=9). CR8 treatment resulted in a significantly reduced number of $GFAP^+$ astrocytes. *$p<0.05$ compared with Sham group (n=3 for Sham groups); #$p<0.05$ compared with SCI Veh group. (**d**) The image shows lesion boundary between spared tissue and lesion cavity, as indicated by GFAP staining. (**e**) Quantification of total Iba-1^+ microglial cells showed significant increase in the injured spinal cord (n=5 for SCI Veh, n=4 for SCI CR8, *$p<0.05$ compared with Sham group), but there is no difference between SCI Veh and SCI CR8 groups. (**f**) Representative Iba-1 immunohistochemical images displayed resting (ramified morphology) or activated (hypertrophic and bushy morphology) microglial phenotypes and the corresponding Neurolucida reconstructions. (**g**, **h**) Unbiased stereological quantitative assessment of microglial phenotypes in the spared tissue and lesion area of the spinal cord 7 days post-injury. There was no significant difference in the number of total microglia and 3 microglial phenotypes in the lesion area, as well as ramified microglia in the spared tissue across groups. CR8 treatment demonstrated significantly reduced numbers of activated microglia in the spared tissue compared with SCI Veh rats (*$p<0.05$ SCI CR8 *vs* SCI Veh; n=4–5/group). GAPDH=glyceraldehyde 3-phosphate dehydrogenase; Gal3=galectin 3

neurons) than in the SCI group that received vehicle treatment (3.5±0.6 Hz, n=33 neurons). Spontaneous firing rates in the SCI vehicle group were significantly different (all $p \leq 0.008$) compared with those in PO neurons from rats that received sham surgery and either CR8 (1.3±0.2 Hz, n=30 neurons) or vehicle treatments (1.6±0.3 Hz, n=24 neurons). CR8 treatment also limited the effects of SCI on evoked responses of PO neurons (Fig. 3b). The magnitude of evoked firing rates was significantly ($p=0.001$) lower in the SCI group that received CR8 (1.5±0.2Hz, n=33 neurons) than in the SCI group that received vehicle treatment (3.4±0.6 Hz, n=34 neurons). Evoked firing in the SCI vehicle group was also significantly different (all $p \leq 0.002$) than those in PO neurons from rats that received sham surgery and either CR8 (1.5±0.2 Hz, n=30 neurons) vehicle treatments (1.3±0.2 Hz, n=24 neurons). The significant negative correlation between firing rate and percent change in baseline mechanical withdrawal threshold was maintained across treatment conditions in this group of animals (spontaneous, Pearson's r=–0.28, $p=0.0017$; sensory-evoked, Pearson's r=–0.27, $p=0.0031$).

These findings support the conclusion that cell cycle inhibition limits the changes in thalamic neuronal excitability in rats with post-traumatic hyperesthesia. That CR8 treatment reduces both SCI-induced hyperesthesia and the associated thalamic changes is consistent with the hypothesis that these PO abnormalities are causally related to the development of post-traumatic hyperpathia

Cell Cycle Inhibition Increases Spared WM Area, Reduces Lesion Volume, and Favors Functional Recovery After SCI

We compared the extent of WM sparing and the volume of spinal lesions in SCI rats that received either CR8 treatment or vehicle injections. Figure 4(a) depicts representative eriochrome stained sections and illustrates the differences in spared WM area between vehicle- and CR8-treated animals. CR8 treatment significantly increased WM area (Fig. 4-b). SCI-induced lesion volume/cavity formation was measured with GFAP/DAB staining 5 weeks after SCI, and analyzed by stereological techniques. There was significantly reduced lesion size and greater preservation of the WM in animals treated with CR8 than in vehicle-treated animals (Fig. 4d). Group analysis showed that lesion volume was significantly smaller in CR8-treated rats (9.63±0.37 mm^3, n=10) compared with that in vehicle-treated controls (15.40±2.00 mm^3, n=8, Fig. 4c). This reduction occurred in both white and gray matter, with an overall decrease in cavity formation and tissue loss. Neurological outcome was also evaluated using the BBB and CBS scores; each test showed significantly improved functional recovery in CR8-treated rats (Fig. 4e, f).

Chronic Microglial Activation Occurs in Selective Thalamic Sites (Including PO) After SCI and is Attenuated by CDK Inhibition

Given that microglial activation in the VPL of the thalamus has been implicated in the development of chronic pain after spinal cord contusion [21], we assessed the potential influence of CDK inhibition on microglial activation of the thalamus following SCI. Immunostaining was performed for inflammatory marker Iba-1 at 7 days and 8 weeks after SCI. Locations of PO and the adjacent nucleus, including the VPM, VPL, and CL in the thalamus, were identified from the Paxinos and Watson atlas (see Fig. 5a). Immunostaining of brain sections from both intact and SCI animals at 7 days post-injury revealed the presence of Iba-1^+ microglia in PO. Importantly, we found a significant increase in the number of these cells in the PO of injured animals compared with sham controls (Fig. 5b). Moreover, the predominant morphotype of microglia in intact tissue displayed small compact cell bodies bearing long thin ramified processes (Fig. 5b (1), c (1)). After SCI, activated Iba-1^+ microglia exhibited larger cell bodies with shorter and thicker projections and retraction of processes at 7 days post-injury (Fig. 5c (2)); these activated microglia occurred not only in PO but also in VPL thalamus. Thus, we confirmed a previous report that activated microglia occur in VPL [21], but demonstrate here that they occur also in "higher order" thalamic nuclei, such as PO. At 8 weeks after injury, activated microglia became progressively

more pronounced in terms of the numbers and pixel intensity (Fig. 5b (3), c(3)), suggesting prolonged activation of microglia in the thalamus. Notably, these changes were significantly attenuated by CR8 treatment (Fig. 5 (d), (e)). We did not observe any significant difference in microglial activation in the adjacent CL nucleus after SCI. Significant increase of the pixel intensity in the VPM was observed at 8 weeks after SCI compared with sham animals, but changes were less than those observed in either the PO or VPL. We did not observe any difference in $GFAP^+$ astrocytes in the PO between intact and SCI animals (data not shown).

SCI-Induced Gliopathy at the Injury Site is Suppressed by CR8 Treatment

Western blot was performed with the 5 mm spinal cord tissue centered on the injury site at 5 weeks after SCI. Expression levels of inflammatory and astrogliosis markers, Iba-1, galectin-3, and GFAP indicated a 3–5-fold increase in injured spinal cord extracts compared with sham tissue (Fig. 6a, b). Stereological assessment of $GFAP^+$ cells showed a 3–4-fold increase from 5 mm caudal to 5 mm rostral the injury epicenter in the injured cords (Fig. 6c). CR8-treated tissue showed significantly reduced levels for these markers in comparison with vehicle-treated tissue (Fig. 6a, b). CR8 treatment significantly reduced the number of $GFAP^+$ cells at 5 weeks post-injury (Fig. 6c). The total number of Iba-1^+ microglial/macrophages was examined at 7 days after SCI when activation of these cells peaks during the early phase of cellular inflammation [25, 63, 64]. SCI caused a 3–4-fold increase of total Iba-1^+ cells; however, such changes were not altered by CR8 treatment (Fig. 6d). Further, we examined activated microglial/macrophages in the preserved tissue, as well as in the central lesion area, where circulating macrophages infiltrate after SCI. Figure 6e shows the lesion boundary between spared tissue and lesion cavity, as indicated by GFAP staining. Representative images and reconstructions (Neurolucida) of the resting (ramified, small cell body with elongated and thin projections) and activated (hypertrophic, large cell body with shorter and thicker projections; bushy, multiple short processes that form thick bundles around enlarged cell bodies) are presented (Fig. 6f). No significant differences were observed in the number of total or ramified microglia across the groups in both spared and lesion areas. Activated microglial phenotypes, including hypertrophic and bushy types, were significantly reduced in the spared tissue in CR8-treated animals compared with vehicle-treated tissue ($p<0.05$). In contrast, CR8 treatment did not significantly affect the number of activated microglial phenotypes in the central lesion area (Fig. 6g, h).

CR8 Administration Reduces Inflammation in the Lumbar Dorsal Horn Following SCI

Microglial activation also contributes to the development and maintenance phases of chronic below-level pain after SCI [28, 65, 66]. To determine if the observed attenuation of below-level mechanical allodynia in CR8-treated rats may be related to the reduced activation of spinal microglial, spinal cord lumbar sections from injured rats perfused at 5 weeks after SCI were stained for ED1/Iba-1, and activated microglia within the superficial dorsal horn were quantified. ED1-positive reactive microglia were rarely seen in uninjured tissue (Fig. 7a), but 5 weeks after SCI, $ED1^+$/Iba-1^+ cells were significantly increased in the injured tissue compared with sham tissue, consistent with other reports [67]. Notably, there was a significant reduction in positively-stained cells in CR8-treated animals (Fig. 7b; $p<0.05$). Thus, decreased numbers of reactive microglia are found in the lumbar spinal dorsal horn in CR8-treated rats associated with reduced below-level mechanical allodynia in these animals.

SCI Causes Up-Regulation of Cyclin D1 and CCL21 Expression in the PO

To further investigate the involvement of the cell cycle pathway in SCI-induced thalamic abnormalities, we first examined whether up-regulation of cell cycle proteins occurs in the thalamus following SCI. Immunohistochemistry was performed to determine the distribution of cyclin D1 in the thalamus following SCI (Fig. 8b, c). In the intact thalamus, immunoreactivity of cyclin D1 was weakly detected in some neurons (Fig. 8a(1)). At 8 weeks post-injury, numerous cyclin D1-positive cells were observed in not only PO (Fig. 8a(2)) but also in VPL (Fig. 8b). Treatment with CR8 revealed a significant reduction of cyclin D1+ cells in these subregions of the thalamus (Fig. 8a(3), b). We did not observe a significant increase in cyclin $D1^+$ cells in the adjacent CL or VPM nuclei (Fig. 8b).

Second, as the neuroimmune modulator CCL21 was reported to be up-regulated in the VPL after SCI and may serve to trigger thalamic microglial activation in association with hyperesthesia [21], we investigated whether CDK inhibitor treatment alters CCL21 levels in PO after SCI. In the intact animal, immunoreactivity of CCL21 was weakly detected (Fig. 8c(1)). At 7 days after SCI, CCL21 immunolabeling showed a clear increase in PO neuronal cell bodies and parenchyma (Fig. 8c(2)). There was a reduction of CCL21 signal at 7 days post-injury in CR8-treated animals (Fig. 8c(3)). Notably, a subset of cyclin $D1^+$ cells were co-labeled with CCL21 (Fig. 8(d)).

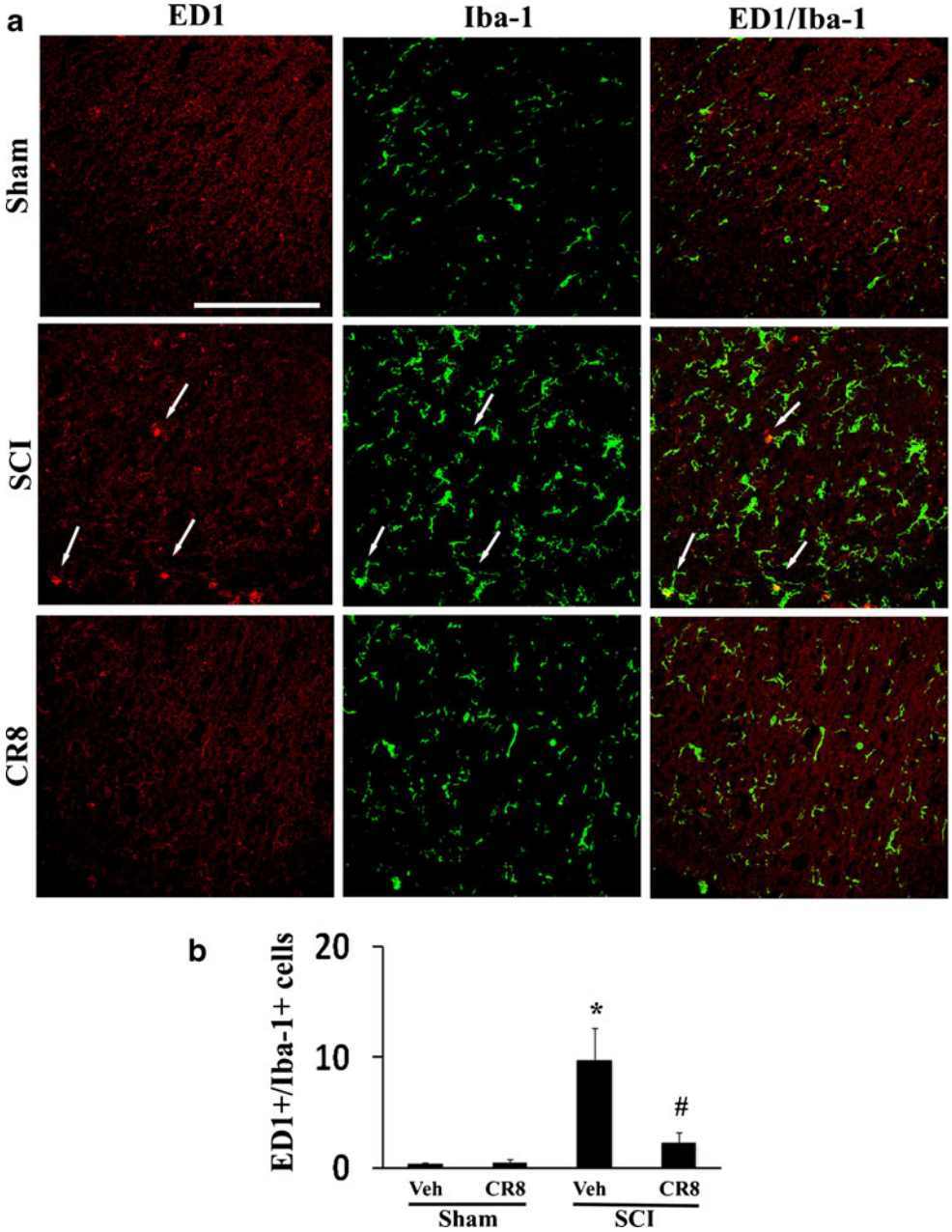

Fig. 7 CR8 administration reduces inflammation in the lumbar dorsal horn following spinal cord injury (SCI). (**a**) Spinal cord lumbar sections from injured rats perfused at 5 weeks were stained with mouse anti-CD68 (ED1)/ ionized calcium-binding adaptor molecule 1 (Iba-1). All images were taken from the superficial dorsal horn. In the sham tissue, no $ED1^+$ microglia cells were observed. After SCI, the number of ED^+/$Iba\text{-}1^+$ microglia (arrows) was increased and attenuated by CR8 treatment. (**b**) Quantification of $ED1^+$-/$Iba\text{-}1^+$-activated microglial cells showed that, after SCI, there are significantly more activated microglia in the lumbar spinal dorsal horn of saline-treated rats (n=7) than in sham animals (n=5, *$p<0.05$). CR8 treatment significantly reduced $ED1^+$-/ $Iba\text{-}1^+$-activated microglial cells [#$p<0.05$ SCI CR8 *vs* SCI vehicle (Veh); n=7/group]. Scale bar=100 μm

Cell Culture Studies

To determine whether increased thalamic levels of cell cycle protein and CCL21 after SCI could be induced by local factors, conditioned medium (CM) from cultured microglia stimulated by LPS or saline were applied to primary neuronal cultures. We observed a significant increase in protein expression of cyclin D1 and CCL21 when the neurons were co-cultured with LPS-treated CM compared with saline-treated CM (Fig. 9a, b). Given that pre-treatment with CDK inhibitors such as flavopiridol and roscovitine significantly reduces microglial proliferation and activation in response to LPS, as indicated by a reduction in NO, we assessed the potency of CR8 compared with earlier purine analogs or flavinoid types of CDK inhibitors [33, 38, 68]. Pre-treatment with CR8 in cultured microglia significantly attenuated LPS-induced microglial proliferation and NO release in a dose-dependent manner (Fig. 9c, d). The effect of CR8 was similar to that of flavopiridol, a potent pan-CDK inhibitor, but with 10–20-fold higher potency than roscovitine, a more selective CDK inhibitor. Importantly, CM from CR8 treatment prior to incubation with LPS significantly reduced protein expression of cyclin D1 and CCL21 compared with the vehicle group (Fig. 9b).

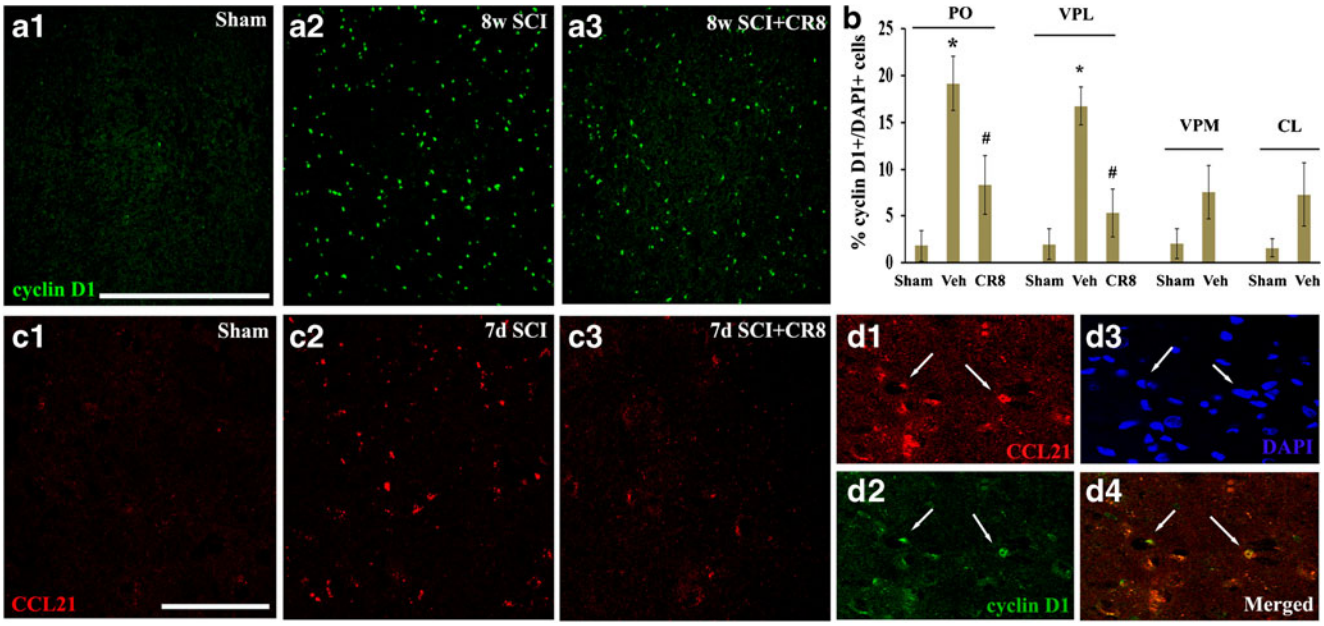

Fig. 8 Expression of cyclin D1 and cysteine–cysteine chemokine ligand 21 (CCL21) was up-regulated in the posterior nucleus (PO) after spinal cord injury (SCI) and reduced by CR8 treatment. (**a**) Cyclin D1 immunostaining revealed weak signal in the PO from sham rats (a1). At 8 weeks post-injury, numerous cyclin D1-positive cells were observed in the PO (a2) and reduced in CR8-treated animals (a3). (**b**) Quantification of percentage of cyclin $D1^+$ cells showed a significant increase in both PO and ventroposteriolateral nucleus (VPL) at 8 weeks (8w) post-injury. Treatment with CR8 revealed a remarkable reduction of cyclin D1 expression in these subregions of the thalamus. We did not observe a significant increase in cyclin $D1^+$ cells in the adjacent centrolateral (CL) or ventral posteromedial (VPM) nucleus. *$p<0.05$ *vs* sham control; #$p<0.05$ *vs* vehicle (Veh) groups. n=3 sections/location/time point/rat for 6–8 rats/group. (**c**) Immunoreactivity of CCL21 was weakly detected in the PO from intact animals (c1). At 7 days (7d) after SCI, CCL21 immunolabeling showed a clear increase in the PO, likely within neuronal cell bodies and parenchyma (c2). Importantly, we observed a reduction of CCL21 signal at 7 days post-injury in CR8-treated animals (c3). (**d**) A subset of cyclin $D1^+$ cells (arrows, green) were co-labeled with CCL21 (arrows, red). Scale bars=500 μm for (**a**) and 100 μm for (**c**) and (**d**). DAPI=4',6-diamidino-2-phenylindole

CR8 Attenuates Up-Regulation of CCA at the Injury Site and in the Lumbar Dorsal Horn After SCI

Quantitative analysis of Western blots showed a marked up-regulation of several key cell cycle proteins, including cyclins D1 and E, CDK4, and PCNA at 5 weeks following SCI (Fig. 10). The up-regulation of cell cycle proteins was significantly attenuated in CR8-treated rats in comparison with vehicle-treated tissue (Fig. 10).

Further, the expression of cell cycle-related proteins was examined in the lumbar spinal dorsal horn by immunohistochemistry. In the intact spinal cord, cyclin D1 was barely detected (Fig. 10g(1)). At 7 days after SCI, cyclin D1 immunoreactivity was up-regulated in the injured tissue (Fig. 10g(2)). CDK4- and E2F1-positive cells were also increased in injured tissue (data not shown). Importantly, the up-regulation of these cell cycle-related proteins was clearly attenuated in the lumbar spinal dorsal horn in rats with CR8 treatment (Fig. 10g(3)).

Discussion

In a rat spinal cord contusion model we show that cell cycle activation contributes to the development of chronic hyperesthesia after SCI, which is closely correlated to increased neuronal activity in the PO nucleus of the thalamus. Up-regulation of cell cycle pathways after SCI occurs not only at the thoracic injury site but also at thalamic pain regulatory sites, including PO and VPL, as well as in the lumbar dorsal horn. Increased CCL21 expression and microglial activation was found in the PO after SCI, and *in vitro* activated microglia up-regulate cell cycle proteins and CCL21 in primary cultured neurons; these changes are suppressed by inhibition of cell cycle activation both *in vivo* and *in vitro*.

Neuronal hyperexcitability in the PO thalamus has been associated with CPS after electrolytic lesions in the ventrolateral quadrant of the spinal cord [24] in which the ascending STT axons degenerate [69]. The PO receives somatosensory inputs from the STT and projects to the primary somatosensory cortex [70–75], which plays an important role in processing sensory-discriminative aspects of pain [76–80]. Here we show that SCI causes significant increases in both spontaneous firing rates and evoked responses in PO neurons, consistent with prior findings after electrolytic lesions of the spinothalamic tract [24]. Moreover, neurons from rats with SCI-related hyperesthesia demonstrate significantly higher neuronal activity than those without hyperesthesia with a significant, negative correlation between firing rates and change in mechanical

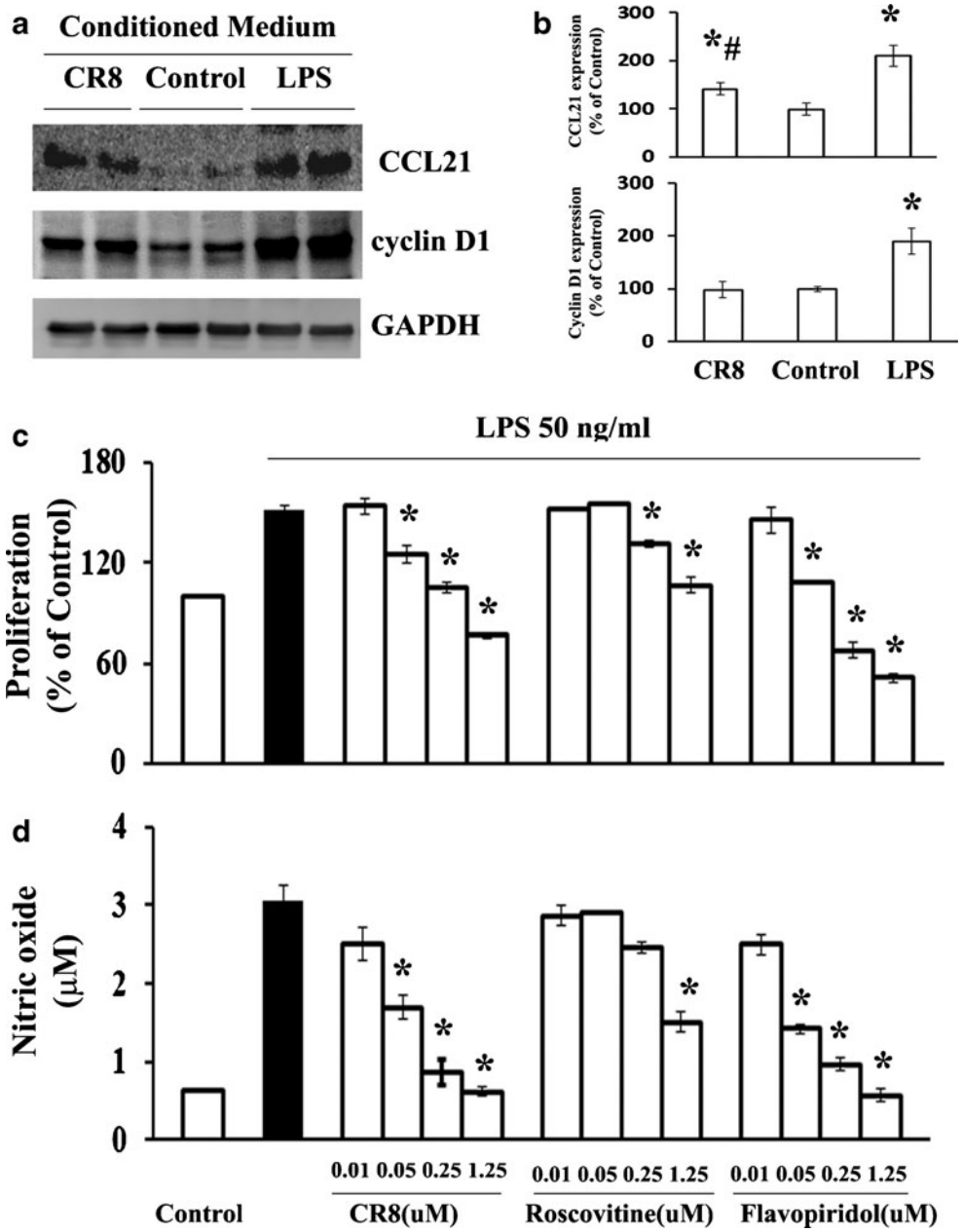

Fig. 9 CR8 potently attenuated up-regulation of cyclin D1 and cysteine–cysteine chemokine ligand 21 (CCL21) expression in cultured neurons stimulated by conditioned medium (CM) derived from lipopolysaccharide (LPS)-activated microglia, as well as microglial proliferation and activation *in vitro*. (**a**, **b**) CM from cultured microglia stimulated by LPS or saline were applied to primary neuronal culture. Protein expression of cyclin D1 and CCL21 was up-regulated when the neurons were co-cultured with LPS-treated CM compared with saline-treated CM (*$p<0.05$ compared with control group, n=4 from 3 independent cultures), and significantly attenuated with CM from CR8 treatment prior to incubation with LPS (#$p<0.05$ compared with LPS group, n=4 from 3 independent cultures). (**c**, **d**) Pre-treatment with CR8 in cultured microglia significantly attenuated LPS-induced both microglial proliferation and release of nitric oxide in a dose-dependent manner. The effect of CR8 was similar to that of flavopiridol, but 10–20-fold higher potency than roscovitine (*$p<0.05$ compared with LPS alone-treated group, n=4 from 4 independent cultures). GAPDH=glyceraldehyde 3-phosphate dehydrogenase

threshold across treatment groups, supporting a causal relation between increases in spontaneous and evoked PO activity and post-SCI hyperesthesia.

SCI-induced neurological effects, including SCI pain, reflect delayed injury-induced processes that contribute to tissue loss and neuroplasticity. These secondary injury processes include neuronal and oligodendroglial cell death, inflammation, and reactive astrogliosis [81, 82]. Post-traumatic CCA has been implicated in delayed neuronal and oligodendroglial apoptosis, reactive astrocytosis and formation of the glial scar, and microglial activation with release of inflammatory factors [34, 83]. Important mediators of CCA are CDKs, a group of small, serine/threonine kinases. We and others have previously found that SCI causes up-regulation of cell cycle pathways, including cyclins and CDKs at the primary lesion site [30, 40, 43, 83, 84]. Here we show that cell cycle proteins are up-regulated not only in the thoracic SCI site and caudal lumbar dorsal horn, but also in the thalamus, suggesting that CCA may contribute to SCI-induced hyperpathia through actions in these areas.

Remote microglial activation has been proposed as a critical mechanism for chronic and persistent pain syndromes after SCI, and in other central pain syndromes [29]. SCI-induced microglial activation in the ventral thalamus has been correlated to lowered nociceptive thresholds through a mechanism involving the chemokine CCL21, a potent microglial activator [21]. Here we report microglial activation in the PO, as well as the VPL after SCI. Whether the microglial changes correlate with the initiation of hyperesthesia could not be

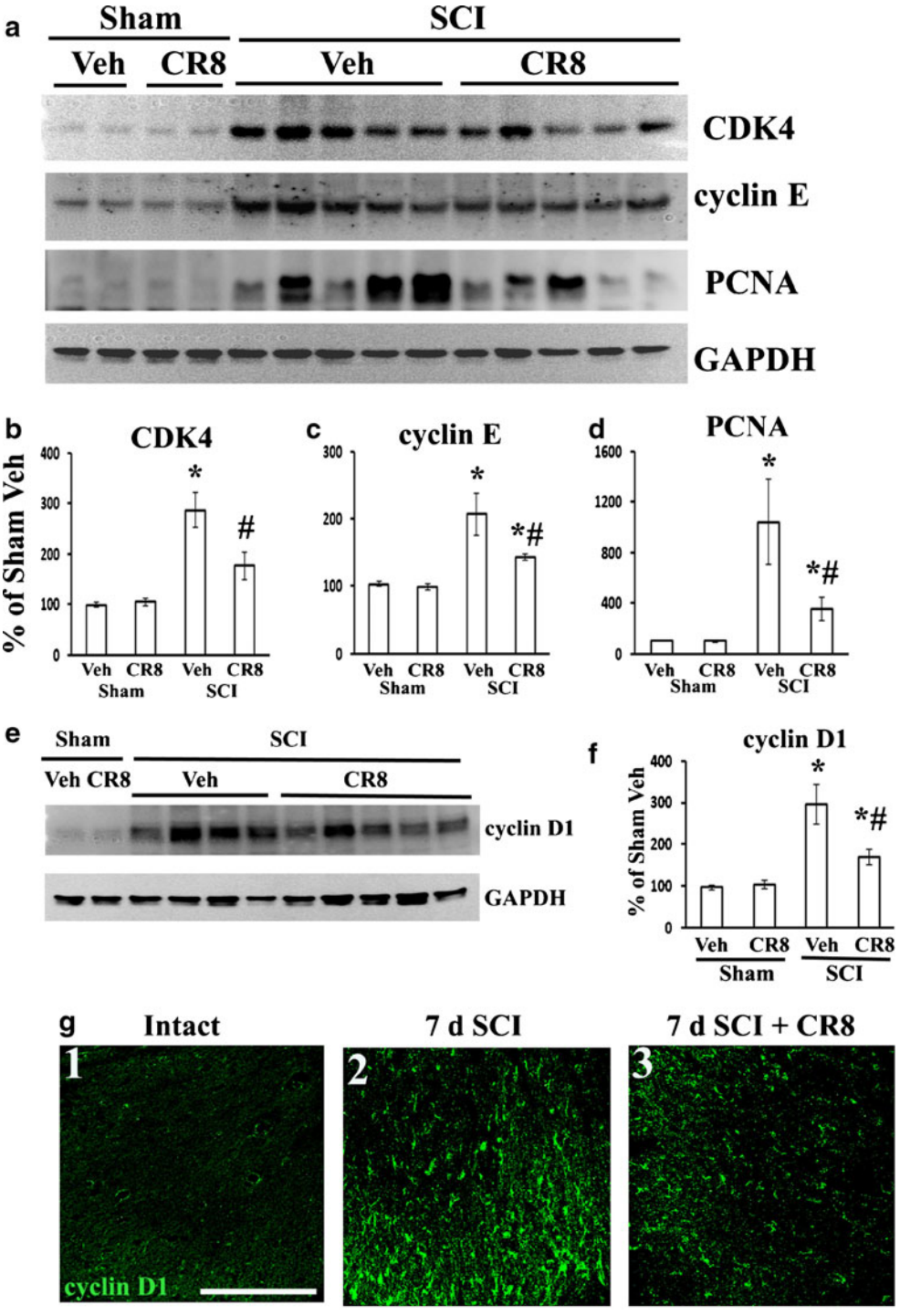

Fig. 10 CR8 attenuates spinal cord injury (SCI)-induced cell cycle activation at the injury site and in the lumbar dorsal horn. (**a**) CR8 attenuated SCI mediated increase in cyclin dependent kinase 4 (CDK4), cyclin E, and PCNA expression at 6 weeks after SCI. (**b**–**d**) Quantification of respective Western blots in panel a. (**e**) CR8 reduced SCI-induced increase in expression of cyclin D1. (**f**) Quantification of Western blot in (**e**). (**g**) Few cyclin $D1^+$ cells were found in the dorsal horn of intact rat (g1). Cyclin $D1^+$ cells increased 7 days after SCI (g2) and was attenuated in CR8-treated animals (g3). Scale bar=100 μm. *$p<0.05$ SCI groups *vs* sham groups; # $p<0.05$ SCI CR8 *vs* SCI vehicle (Veh); n=4–5/group. GAPDH=glyceraldehyde 3-phosphate dehydrogenase. *PCNA* proliferating cell nuclear antigen

determined because before 4 weeks post-injury reliable somatosensory testing is not possible owing to locomotor deficits that preclude testing of nociceptive thresholds. CCL21 levels were also elevated in the PO at 7 days post-SCI, and partly co-labeled with cyclin D1. It is possible that CCL21 activates resident microglia in the PO, which contributes to the nociceptive effects mediated by neuronal activity in this region. CCL21 signal was increased in cultured neurons exposed to high concentrations of glutamate [85] and in excitatory neurons of the dorsal horn, and in spinal parenchyma after SCI [21]. Here we show that CM derived from activated microglia *in vitro* induces CCL21, as well as cell cycle protein expression in cultured neurons, suggesting that the increased CLL21 levels in the thalamus after SCI may, in part, reflect the observed local microglial activation. This conclusion would be consistent with the report of Zhao et al. [21] showing that CCL21 levels were not completely abolished by cord transection rostral to both the injury site and lumbar enlargement after SCI. Thus, CCL21

may be an important source, at least in part, for chronic thalamic microglial activation that maintains thalamic neuronal hyperactivity associated with persistent SCI pain. Cell cycle inhibition by CR8 decreased CCL21 levels in the PO after SCI, as well as in cultured neurons exposed to effluent from LPS-treated microglia. Further investigation is required to elucidate the mechanisms by which cell cycle inhibition modulates CCL21 signals after SCI.

SCI-induced astrogliosis and chronic inflammation in the lesion site are believed to contribute to glial scar formation and the progressive spinal cord tissue loss (including the WM that contains the STT) [30, 64, 86]. Our findings demonstrate that the selective and potent CDK inhibitor, CR8, significantly attenuates secondary tissue damage and related neurological dysfunction after impact spinal cord trauma, consistent with prior work demonstrating the neuroprotective effects of other cell cycle inhibitors after SCI [34, 43, 84]. CR8 significantly attenuated activated microglial phenotypes in the spared tissue and increased WM sparing including the ventrolateral quadrant that contains the STT. To what extent this effect serves to modulate post-injury hyperesthesia is speculative, but multisegmental anti-inflammatory actions at both caudal and supratentorial sites likely contributes to the striking ability of CDK inhibition to limit post-traumatic hyperesthesia.

Gliopathy in the lumbar dorsal horn may serve to maintain hyperexcitability of nociceptive neurons associated with hyperesthesia that follows SCI [28]. Thus, both spinal and thalamic mechanisms may be important in the genesis of pain and allodynia following SCI. We have previously demonstrated that treatment with cell cycle inhibitors markedly reduces chronic post-traumatic microglial activation at lesion sites. Here, we show, for the first time, that CCA contributes to *remote* microglial activation after SCI, including the thalamus and lumbar spinal dorsal horn, as evidenced by reduction of microglia activation in these areas following CCA inhibition. CR8 limited the development of hyperesthesia after SCI with an associated reduction in neuronal activity in the PO. These effects may reflect suppression of microglial activation that may contribute to changes in thalamic plasticity after injury. Microglia have multiple phenotypes: M1 is associated with cytokine release and neurotoxicity; M2 can modulate neuroplasticity. To what extent the ability of the CDK inhibition to reduce post-traumatic thalamic plasticity reflect its effects on M1 or M2 phenotypes requires further study.

Together, our data suggest that neurophysiological changes in the PO thalamus may contribute to SCI pain. These effects appear to be mediated in part by CCA, which may also contribute to post-injury hyperesthesia by mediating astroglial and microglial actions in the spinal cord. Given the proposed roles for CCA in other neuropathic pain models, it is plausible that activation of cell cycle pathways also represents a more generic mechanism relevant to other neuropathic pain states.

Acknowledgments This study was supported by the National Institutes of Health Grants R01 NS054221 (AIF) and R01 NS066965 (AK). We thank Michael Dinizo, Kelsey Guanciale, Rainier Cabatbat, Katherine Cardiff, Marie Hanscom, Angela Pan, and Aicha Moutanni for expert technical support.

Required Author Forms Disclosure forms provided by the authors are available with the online version of this article.

Conflict of Interest The authors declare that they have no competing financial interests.

References

1. Persu C, Caun V, Dragomiriteanu I, Geavlete P. Urological management of the patient with traumatic spinal cord injury. J Med Life 2009;2:296-302.
2. Widerstrom-Noga EG, Felix ER, Cruz-Almeida Y, Turk DC. Psychosocial subgroups in persons with spinal cord injuries and chronic pain. Arch Phys Med Rehabil 2007;88:1628-1635.
3. Abramson CE, McBride KE, Konnyu KJ, Elliott SL. Sexual health outcome measures for individuals with a spinal cord injury: a systematic review. Spinal Cord 2008;46:320-324.
4. Stormer S, Gerner HJ, Gruninger W, et al. Chronic pain/dysaesthesiae in spinal cord injury patients: results of a multicentre study. Spinal Cord 1997;35:446-455.
5. Yezierski RP. Pain following spinal cord injury: pathophysiology and central mechanisms. Prog Brain Res 2000;129:429-449.
6. Defrin R, Ohry A, Blumen N, Urca G. Pain following spinal cord injury. Spinal Cord 2002;40:96-97.
7. Tasker RR. Meralgia paresthetica. J Neurosurg 1991;75:168.
8. Greenspan JD, Ohara S, Sarlani E, Lenz FA. Allodynia in patients with post-stroke central pain (CPSP) studied by statistical quantitative sensory testing within individuals. Pain 2004;109:357-366.
9. Baastrup C, Finnerup NB. Pharmacological management of neuropathic pain following spinal cord injury. CNS Drugs 2008;22:455-475.
10. Tasker RR, DeCarvalho GT, Dolan EJ. Intractable pain of spinal cord origin: clinical features and implications for surgery. J Neurosurg 1992;77:373-378.
11. Falci S, Best L, Bayles R, Lammertse D, Starnes C. Dorsal root entry zone microcoagulation for spinal cord injury-related central pain: operative intramedullary electrophysiological guidance and clinical outcome. J Neurosurg 2002;97:193-200.
12. Rintala DH, Holmes SA, Fiess RN, Courtade D, Loubser PG. Prevalence and characteristics of chronic pain in veterans with spinal cord injury. J Rehabil Res Dev 2005;42:573-584.
13. Masri R, Keller A. Chronic pain following spinal cord injury. Adv Exp Med Biol 2012;760:74-88.
14. Lenz FA, Kwan HC, Dostrovsky JO, Tasker RR. Characteristics of the bursting pattern of action potentials that occurs in the thalamus of patients with central pain. Brain Res 1989;496:357-360.
15. Yezierski RP. Spinal cord injury pain: spinal and supraspinal mechanisms. J Rehab Res Develop 2009;46:95-107.
16. Waxman SG, Hains BC. Fire and phantoms after spinal cord injury: Na+ channels and central pain. Trends Neurosci 2006;29:207-215.
17. Hubscher CH, Johnson RD. Chronic spinal cord injury induced changes in the responses of thalamic neurons. Exp Neurol 2006;197:177-188.
18. Gerke MB, Duggan AW, Xu L, Siddall PJ. Thalamic neuronal activity in rats with mechanical allodynia following contusive spinal cord injury. Neuroscience 2003;117:715-722.

19. Hains BC, Saab CY, Waxman SG. Changes in electrophysiological properties and sodium channel Nav1.3 expression in thalamic neurons after spinal cord injury. Brain 2005;128:2359-2371.
20. Hains BC, Saab CY, Waxman SG. Alterations in burst firing of thalamic VPL neurons and reversal by Na(v)1.3 antisense after spinal cord injury. J Neurophysiol 2006;95:3343-3352.
21. Zhao P, Waxman SG, Hains BC. Modulation of thalamic nociceptive processing after spinal cord injury through remote activation of thalamic microglia by cysteine cysteine chemokine ligand 21. J Neurosci 2007;27:8893-8902.
22. Poggio GF, Mountcastle VB. A study of the functional contributions of the lemniscal and spinothalamic systems to somatic sensibility. Central nervous mechanisms in pain. Bull Johns Hopkins Hosp 1960;106:266-316.
23. Zhang X, Giesler GJ, Jr. Response characteristics of spinothalamic tract neurons that project to the posterior thalamus in rats. J Neurophysiol 2005;93:2552-2564.
24. Masri R, Quiton RL, Lucas JM, Murray PD, Thompson SM, Keller A. Zona incerta: a role in central pain. J Neurophysiol 2009;102:181-191.
25. Popovich PG, Wei P, Stokes BT. Cellular inflammatory response after spinal cord injury in Sprague-Dawley and Lewis rats. J Comp Neurol 1997;377:443-464.
26. Schmitt AB, Buss A, Breuer S, et al. Major histocompatibility complex class II expression by activated microglia caudal to lesions of descending tracts in the human spinal cord is not associated with a T cell response. Acta Neuropathol 2000;100:528-536.
27. Crown ED, Ye Z, Johnson KM, Xu GY, McAdoo DJ, Hulsebosch CE. Increases in the activated forms of ERK 1/2, p38 MAPK, and CREB are correlated with the expression of at-level mechanical allodynia following spinal cord injury. Exp Neurol 2006;199:397-407.
28. Hains BC, Waxman SG. Activated microglia contribute to the maintenance of chronic pain after spinal cord injury. J Neurosci 2006;26:4308-4317.
29. Hulsebosch CE, Hains BC, Crown ED, Carlton SM. Mechanisms of chronic central neuropathic pain after spinal cord injury. Brain Res Rev 2009;60:202-213.
30. Wu J, Pajoohesh-Ganji A, Stoica BA, Dinizo M, Guanciale K, Faden AI. Delayed expression of cell cycle proteins contributes to astroglial scar formation and chronic inflammation after rat spinal cord contusion. J Neuroinflammation 2012;9:169.
31. Gwak YS, Kim HK, Kim HY, Leem JW. Bilateral hyperexcitability of thalamic VPL neurons following unilateral spinal injury in rats. J Physiol Sci 2010;60:59-66.
32. Hulsebosch CE. Gliopathy ensures persistent inflammation and chronic pain after spinal cord injury. Exp Neurol 2008;214:6-9.
33. Di Giovanni S, Movsesyan V, Ahmed F, et al. Cell cycle inhibition provides neuroprotection and reduces glial proliferation and scar formation after traumatic brain injury. Proc Natl Acad Sci U S A 2005;102:8333-8338.
34. Wu J, Stoica BA, Faden AI. Cell cycle activation and spinal cord injury. Neurotherapeutics 2011;8:221-228.
35. Osuga H, Osuga S, Wang F, et al. Cyclin-dependent kinases as a therapeutic target for stroke. Proc Natl Acad Sci U S A 2000;97:10254-10259.
36. Park DS, Morris EJ, Bremner R, et al. Involvement of retinoblastoma family members and E2F/DP complexes in the death of neurons evoked by DNA damage. J Neurosci 2000;20:3104-3114.
37. Wang F, Corbett D, Osuga H, et al. Inhibition of cyclin-dependent kinases improves CA1 neuronal survival and behavioral performance after global ischemia in the rat. J Cereb Blood Flow Metab 2002;22:171-182.
38. Cernak I, Stoica B, Byrnes KR, Di Giovanni S, Faden AI. Role of the cell cycle in the pathobiology of central nervous system trauma. Cell Cycle 2005;4:1286-1293.
39. Byrnes KR, Stoica BA, Fricke S, Di Giovanni S, Faden AI. Cell cycle activation contributes to post-mitotic cell death and secondary damage after spinal cord injury. Brain 2007;130:2977-2992.
40. Tian DS, Dong Q, Pan DJ, et al. Attenuation of astrogliosis by suppressing of microglial proliferation with the cell cycle inhibitor olomoucine in rat spinal cord injury model. Brain Res 2007;1154:206-214.
41. Liu DZ, Ander BP, Sharp FR. Cell cycle inhibition without disruption of neurogenesis is a strategy for treatment of central nervous system diseases. Neurobiol Dis 2010;37:549-557.
42. Kabadi SV, Stoica BA, Byrnes KR, Hanscom M, Loane DJ, Faden AI. Selective CDK inhibitor limits neuroinflammation and progressive neurodegeneration after brain trauma. J Cereb Blood Flow Metab 2012;32:137-149.
43. Wu J, Stoica BA, Dinizo M, Pajoohesh-Ganji A, Piao C, Faden AI. Delayed cell cycle pathway modulation facilitates recovery after spinal cord injury. Cell Cycle 2012;11:1782-1795.
44. Tsuda M, Kohro Y, Yano T, et al. JAK-STAT3 pathway regulates spinal astrocyte proliferation and neuropathic pain maintenance in rats. Brain 2011;134:1127-1139.
45. Wang CH, Chou WY, Hung KS, et al. Intrathecal administration of roscovitine inhibits Cdk5 activity and attenuates formalin-induced nociceptive response in rats. Acta Pharmacol Sin 2005;26:46-50.
46. Yang YR, He Y, Zhang Y, et al. Activation of cyclin-dependent kinase 5 (Cdk5) in primary sensory and dorsal horn neurons by peripheral inflammation contributes to heat hyperalgesia. Pain 2007;127:109-120.
47. Yakovlev AG, Faden AI. Sequential expression of c-fos protooncogene, TNF-alpha, and dynorphin genes in spinal cord following experimental traumatic injury. Mol Chem Neuropathol 1994;23:179-190.
48. Basso DM, Beattie MS, Bresnahan JC. A sensitive and reliable locomotor rating scale for open field testing in rats. J Neurotrauma 1995;12:1-21.
49. Gale K, Kerasidis H, Wrathall JR. Spinal cord contusion in the rat: behavioral analysis of functional neurologic impairment. Exp Neurol 1985;88:123-134.
50. Trageser JC, Burke KA, Masri R, Li Y, Sellers L, Keller A. State-dependent gating of sensory inputs by zona incerta. J Neurophysiol 2006;96:1456-1463.
51. Sceniak MP, Maciver MB. Cellular actions of urethane on rat visual cortical neurons in vitro. J Neurophysiol 2006;95:3865-3874.
52. Friedberg MH, Lee SM, Ebner FF. Modulation of receptive field properties of thalamic somatosensory neurons by the depth of anesthesia. J Neurophysiol 1999;81:2243-2252.
53. West MJ, Slomianka L, Gundersen HJ. Unbiased stereological estimation of the total number of neurons in thesubdivisions of the rat hippocampus using the optical fractionator. Anat Rec 1991;231:482-497.
54. Soltys Z, Ziaja M, Pawlinski R, Setkowicz Z, Janeczko K. Morphology of reactive microglia in the injured cerebral cortex. Fractal analysis and complementary quantitative methods. J Neurosci Res 2001;63:90-97.
55. Byrnes KR, Loane DJ, Stoica BA, Zhang J, Faden AI. Delayed mGluR5 activation limits neuroinflammation and neurodegeneration after traumatic brain injury. J Neuroinflammation 2012;9:43.
56. Wu J, Kharebava G, Piao C, et al. Inhibition of E2F1/CDK1 pathway attenuates neuronal apoptosis in vitro and confers neuroprotection after spinal cord injury in vivo. PLoS One 2012;7:e42129.
57. Lee HJ, Wu J, Chung J, Wrathall JR. SOX2 expression is upregulated in adult spinal cord after contusion injury in both oligodendrocyte lineage and ependymal cells. J Neurosci Res 2013;91:196-210.
58. Wu J, Wrathall JR, Schachner M. Phosphatidylinositol 3-kinase/protein kinase Cdelta activation induces close homolog of adhesion molecule L1 (CHL1) expression in cultured astrocytes. Glia 2010;58:315-328.

59. Hubscher CH, Fell JD, Gupta DS. Sex and hormonal variations in the development of at-level allodynia in a rat chronic spinal cord injury model. Neurosci Lett 2010;477:153-156.
60. Hall BJ, Lally JE, Vukmanic EV, et al. Spinal cord injuries containing asymmetrical damage in the ventrolateral funiculus is associated with a higher incidence of at-level allodynia. J Pain 2010;11:864-875.
61. Whitt JL, Masri R, Pulimood NS, Keller A. Pathological activity in mediodorsal thalamus of rats with spinal cord injury pain. J Neurosci 2013;33:3915-3926.
62. Vierck CJ, Jr., Siddall P, Yezierski RP. Pain following spinal cord injury: animal models and mechanistic studies. Pain 2000;89:1-5.
63. Carlson SL, Parrish ME, Springer JE, Doty K, Dossett L. Acute inflammatory response in spinal cord following impact injury. Exp Neurol 1998;151:77-88.
64. Beck KD, Nguyen HX, Galvan MD, Salazar DL, Woodruff TM, Anderson AJ. Quantitative analysis of cellular inflammation after traumatic spinal cord injury: evidence for a multiphasic inflammatory response in the acute to chronic environment. Brain 2010;133:433-447.
65. Detloff MR, Fisher LC, McGaughy V, Longbrake EE, Popovich PG, Basso DM. Remote activation of microglia and pro-inflammatory cytokines predict the onset and severity of below-level neuropathic pain after spinal cord injury in rats. Exp Neurol 2008;212:337-347.
66. Ji RR, Kawasaki Y, Zhuang ZY, Wen YR, Decosterd I. Possible role of spinal astrocytes in maintaining chronic pain sensitization: review of current evidence with focus on bFGF/JNK pathway. Neuron Glia Biol 2006;2:259-269.
67. Gwak YS, Kang J, Unabia GC, Hulsebosch CE. Spatial and temporal activation of spinal glial cells: role of gliopathy in central neuropathic pain following spinal cord injury in rats. Exp Neurol 2012;234:362-372.
68. Hilton GD, Stoica BA, Byrnes KR, Faden AI. Roscovitine reduces neuronal loss, glial activation, and neurologic deficits after brain trauma. J Cereb Blood Flow Metab 2008;28:1845-1859.
69. Wang G, Thompson SM. Maladaptive homeostatic plasticity in a rodent model of central pain syndrome: thalamic hyperexcitability after spinothalamic tract lesions. J Neurosci 2008;28:11959-11969.
70. Koralek KA, Jensen KF, Killackey HP. Evidence for two complementary patterns of thalamic input to the rat somatosensory cortex. Brain Res 1988;463:346-351.
71. Nothias F, Peschanski M, Besson JM. Somatotopic reciprocal connections between the somatosensory cortex and the thalamic Po nucleus in the rat. Brain Res 1988;447:169-174.
72. Chmielowska J, Carvell GE, Simons DJ. Spatial organization of thalamocortical and corticothalamic projection systems in the rat SmI barrel cortex. J Comp Neurol 1989;285:325-338.
73. Fabri M, Burton H. Topography of connections between primary somatosensory cortex and posterior complex in rat: a multiple fluorescent tracer study. Brain Res 1991;538:351-357.
74. Lu SM, Lin RC. Thalamic afferents of the rat barrel cortex: a light- and electron-microscopic study using Phaseolus vulgaris leucoagglutinin as an anterograde tracer. Somatosens Mot Res 1993;10:1-16.
75. Bureau I, von Saint Paul F, Svoboda K. Interdigitated paralemniscal and lemniscal pathways in the mouse barrel cortex. PLoS Biol 2006;4:e382.
76. Bushnell MC, Duncan GH, Hofbauer RK, Ha B, Chen JI, Carrier B. Pain perception: is there a role for primary somatosensory cortex? Proc Natl Acad Sci U S A 1999;96:7705-7709.
77. Coghill RC, Sang CN, Maisog JM, Iadarola MJ. Pain intensity processing within the human brain: a bilateral, distributed mechanism. J Neurophysiol 1999;82:1934-1943.
78. Apkarian AV, Bushnell MC, Treede RD, Zubieta JK. Human brain mechanisms of pain perception and regulation in health and disease. Eur J Pain 2005;9:463-484.
79. Moulton EA, Keaser ML, Gullapalli RP, Greenspan JD. Regional intensive and temporal patterns of functional MRI activation distinguishing noxious and innocuous contact heat. J Neurophysiol 2005;93:2183-2193.
80. Quiton RL, Masri R, Thompson SM, Keller A. Abnormal activity of primary somatosensory cortex in central pain syndrome. J Neurophysiol 2010;104:1717-1725.
81. Tator CH, Fehlings MG. Review of clinical trials of neuroprotection in acute spinal cord injury. Neurosurg Focus 1999;6:e8.
82. Dumont RJ, Okonkwo DO, Verma S, et al. Acute spinal cord injury, part I: pathophysiologic mechanisms. Clin Neuropharmacol 2001;24:254-264.
83. Di Giovanni S, Knoblach SM, Brandoli C, Aden SA, Hoffman EP, Faden AI. Gene profiling in spinal cord injury shows role of cell cycle in neuronal death. Ann Neurol 2003;53:454-468.
84. Byrnes KR, Faden AI. Role of cell cycle proteins in CNS injury. Neurochem Res 2007;32:1799-1807.
85. de Jong EK, Dijkstra IM, Hensens M, et al. Vesicle-mediated transport and release of CCL21 in endangered neurons: a possible explanation for microglia activation remote from a primary lesion. J Neurosci 2005;25:7548-7557.
86. Byrnes KR, Washington PM, Knoblach SM, Hoffman E, Faden AI. Delayed inflammatory mRNA and protein expression after spinal cord injury. J Neuroinflammation 2011;8:130.
87. Paxinos G, Watson C. The rat brain in stereotaxic coordinates (2nd edn). Academic Press, Inc., 1998, plate 29.